https://doi.org/10.5194/egusphere-2025-1776
Preprint. Discussion started: 13 May 2025

Measurement Report: Optical properties of supermicron aerosol particles in a boreal environment

Sujai Banerji[1], Krista Luoma[2], Ilona Ylivinkka[1], Lauri Ahonen[1], Veli-Matti Kerminen[1], and Tuukka Petäjä[1]

[1]Institute for Atmospheric and Earth System Research (INAR)/Physics, Faculty of Science, University of Helsinki, Helsinki, Finland

[2]Finnish Meteorological Institute, Helsinki, Finland

Correspondence to: Sujai Banerji (sujai.banerji@helsinki.fi)

Abstract

Supermicron aerosol particles ($PM_{1\text{-}10}$; here defined as 1 µm < aerodynamic diameter, 10 µm) play a crucial role in aerosol-climate interactions by influencing light scattering and absorption. However, their long-term trends and episodic significance in boreal environments remain insufficiently understood. This study examines measurements of optical properties and mass of $PM_{1\text{-}10}$ over a 12-year period at the SMEAR II station in Hyytiälä, Finland, focusing on their variability and key drivers. By assessing long-term trends, seasonality, and episodic variability, the study provides new insights into the role of these particles in aerosol-climate interactions. Episodic events, such as pollen outbreaks and dust transport, are identified as major contributors to $PM_{1\text{-}10}$ variability and their role in atmospheric processes. In addition, cascade impactor filters were used to quantify super-PM_{10} particles (D_p > 10 µm), which are not detected by optical instruments, addressing key detection limitations. The findings reveal significant long-term trends and pronounced seasonality in $PM_{1\text{-}10}$ mass and optical properties, emphasizing their importance in boreal environments and their episodic relevance in coarse-mode aerosol characterization.

1. Introduction

Aerosols are integral to atmospheric processes, influencing climate, air quality, and radiative forcing. Among them, coarse-mode aerosol particles, which are typically defined as particles with diameters > 1 µm play a significant role in light scattering and absorption, directly impacting radiative forcing. Their size and optical properties make them dominant contributors to aerosol optical depth (AOD), particularly at longer wavelengths. Coarse-mode aerosol particles, such as biological aerosols found in the boreal environment, also contribute to cloud microphysics by serving as ice-nucleating particles (Brasseur et al., 2022). Despite their importance, the optical properties and particulate matter mass (PM mass) of coarse-mode aerosol particles remain understudied (Cappa et al., 2016).

Boreal forests, covering approximately 15% of the Earth's terrestrial surface, represent a unique natural laboratory for studying aerosol-climate interactions in biogenically dominated environments. These ecosystems emit large quantities of biogenic volatile organic compounds (BVOCs; Guenther et al. (2006)), which drive the formation of secondary organic aerosols (SOA), significantly influencing aerosol size distribution and, therefore, light

https://doi.org/10.5194/egusphere-2025-1776
Preprint. Discussion started: 13 May 2025

scattering and absorption processes (Petäjä et al., 2022; Tunved et al., 2006). Additionally, episodic events such as pollen outbreaks and long-range transport of mineral dust contribute to aerosol variability in boreal regions (Manninen et al., 2014).

Coarse-mode particles in boreal environments are dominantly primary aerosol particles—particles emitted directly into the atmosphere rather than formed through chemical reactions. These include dust, pollen, fungal spores, plant debris, and sea salt, as well as particles from episodic sources like wildfires or small-scale wood combustion, which could explain higher concentrations in winter. Mineral dust is typically transported long distances, while pollen and spores often originate from more local biogenic emissions that are highly episodic and seasonal. Sea salt, though typically associated with marine environments, can occasionally reach boreal forests during strong winds. Wildfire emissions, though predominantly in the fine mode, can contain coarse-mode particles, particularly in smoldering phases or from ash deposition.

The size fractions of these coarse-mode particles range from 1 µm to over 10 µm. Pollen grains and larger fungal spores often exceed the PM_{10} cut-off and may not be fully captured by standard PM_{10} measurements, leaving their contributions underrepresented in coarse-mode analyses. Understanding the extent to which these particles are detected or left out of PM_{10} measurements is crucial for characterizing their impacts.

The natural components of coarse-mode aerosol particles contribute to atmospheric heterogeneity, influencing key microphysical processes, such as the activation of ice-nucleating particles (INPs), and playing a vital role in atmospheric processes like cloud formation, nutrient cycling, and radiative interactions (Brasseur et al., 2024; Després et al., 2012; Mahowald et al., 2014; Schneider et al., 2021). Despite their recognized importance, the interactions between these natural components and atmospheric dynamics in boreal environments remain poorly characterized, particularly in the context of episodic events like pollen releases, dust transport, and potential contributions from biomass burning.

The coarse-mode size range also presents challenges for optical instruments, with upper size cut-offs typically set to 10 µm, potentially leaving a significant fraction of aerosol mass unquantified (Zieger et al., 2015). This undetected mass fraction is crucial for achieving optical closure and improving vertical column density estimates in boreal environments. Furthermore, the detection of coarse-mode particles depends on their size: particles larger than 10 µm, such as pollen, may escape standard measurements, whereas smaller coarse-mode particles, such as fungal spores and dust, are more likely to be captured.

The knowledge gaps regarding coarse-mode aerosol particles hinder our ability to fully understand their optical and mass properties and their contributions to regional and global atmospheric processes. Addressing these gaps requires a detailed investigation that accounts for both long-term trends and episodic variability. Our study offers a comprehensive analysis, focusing on the optical properties and PM mass of $PM_{1\text{-}10}$ aerosol particles, from the SMEAR II station in Hyytiälä, Finland, to improve the understanding of the sources, behavior, and impacts of $PM_{1\text{-}10}$ aerosol particles, which is essential for advancing knowledge of their role in atmospheric and climatic processes. While this study focuses on $PM_{1\text{-}10}$ particles, it also examines the PM mass of super-PM_{10} particles using gravimetric analysis of cascade impactor filters. Specifically, this study aims to:

https://doi.org/10.5194/egusphere-2025-1776
Preprint. Discussion started: 13 May 2025

(a) Investigate the measurements of optical properties and mass of PM_{1-10} aerosol particles at the SMEAR II station to analyze long-term trends of coarse-mode aerosol particles and their variability in boreal environments.

(b) Quantify the PM mass fraction of coarse-mode aerosol particles beyond the detection limits of optical instruments, constrained by the 10 µm size cut-off (super-PM_{10}), with implications for optical closure and vertical column density estimates.

(c) Assess the statistical significance of episodic events, such as pollen outbreaks and dust transport, on the optical properties of PM_{1-10} aerosol particles.

(d) Examine the PM mass of the super-PM_{10} aerosol particles to fully capture the contributions of larger particles and their episodical significance in events such as pollen outbreaks or dust transport.

2. Measurement and methods

2.1 SMEAR II

The Station for Measuring Ecosystem–Atmosphere Relations (SMEAR II) is located in Hyytiälä, southern Finland (61°51'N, 24°17'E; 181 m.a.s.l.). It is located in a boreal forest and is classified as a background site where no major local sources of aerosol particles from anthropogenic activities are observed (Hari & Kulmala, 2005). However, there are some sources of pollution in the region, such as the city of Tampere (60 km in the southwest direction with a population of 241,000 in 2021) and the activity of the buildings in the station (Boy, 2004; Kulmala et al., 2001). Thus, SMEAR II represents the typical conditions that may be found in a boreal forest (Hari et al., 2013). It has instruments to measure interactions between the forest ecosystem and the atmosphere. It is a part of the European Aerosols, Clouds, and Trace Gases Research Infrastructure or ACTRIS (Laj et al., 2024). The station has various aerosol instruments, including the three instruments used in this study: a Magee Scientific aethalometer (models AE31 and AE33) to obtain the light absorption coefficient at seven wavelengths, a TSI integrating nephelometer (model 3563) to calculate the light scattering coefficient at three wavelengths and a Dekati cascade gravimetric impactor to measure the PM mass of different size fractions (i.e. $\leq PM_1$, $\leq PM_1$-$PM_{2.5}$, $\leq PM_{2.5}$-PM_{10}, $\leq PM_{10}$, $> PM_{10}$). The instruments are described in more detail in the following sections. All these instruments are in a *'Hitumökki,'* i.e., the 'Aerosol Cottage'.

2.2 Measurement setup and instruments

The measurement setup for the aerosol optical instruments included a pre-impactor designed to remove the aerosol particles with an D_p >10 µm sampling PM_{10} aerosol particles. The inlet is located at a height of 8 m above ground inside the forest canopy. Following the pre-impactor, the airflow sequentially passed through an inlet flow splitter. This configuration allowed us to sample aerosol particles with aerodynamic diameter <1 µm (hereafter PM_1 aerosol particles) or PM_{10} every ten minutes. The switching inlet system has been described in detail by Luoma et al. (2021). Subsequently the size selected sample with a flow rate of 30 l min^{-1} is split into three streams to optical instruments.

https://doi.org/10.5194/egusphere-2025-1776
Preprint. Discussion started: 13 May 2025

One of the airstreams from the splitter goes into a Nafion dryer connected to an integrating nephelometer (TSI model 3563). With the Nafion dryer, the relative humidity of the sampled air is aimed be kept below 40%. The integrating nephelometer maintains a flow rate of 8.3 l min^{-1}.

The second airstream from the splitter passes through a different Nafion dryer and then enters the Magee Scientific aethalometer (models AE31 and AE33). The AE31 operated at SMEAR II until December 2017 and was replaced by the newer model AE33 in February 2018. The aethalometers maintain a flow rate of 5 l min^{-1}.

The third airstream is directed into a Thermo Fischer multi-angle absorption photometer (MAAP; model 5012) through a Nafion dryer. The MAAP maintains the flow rate of 16.7 l min^{-1}.

2.2.1 Aethalometer

The aethalometer quantifies the aerosol absorption coefficient (σ_{abs}) by measuring the reduction in light intensity as particles collect on a filter, facilitating continuous aerosol sampling (Zotter et al., 2017). The AE31 and AE33 models compare photon counts from light transmitted through a particle-laden filter spot to a clean reference filter. Correction algorithms account for aerosol particle scattering and multiple scattering within the quartz fiber filter. As light-absorbing particles build up, the effective optical path length shortens, necessitating adjustments for the filter-loading effect (Collaud Coen et al., 2010; Weingartner et al., 2003). The multiple-scattering correction factor (C_{ref}) addresses the enhancement of light scattering within the filter matrix due to the filter material, while the filter loading correction factor (*R(ATN)*) accounts for the non-linear instrument response caused by particle accumulation on the filter (Liousse et al., 1993). Further refinement in measurement accuracy is achieved by using single-scattering albedo (ω_0), which combines scattering and absorption coefficients to enhance the characterization of aerosol properties (Weingartner et al., 2003).

The Magee Scientific AE31 Aethalometer was operated at SMEAR II from October 2010 to December 2017 for continuous measurements of σ_{abs} at seven discrete wavelengths between 370 and 950 nm. Due to the single-spot filter design of the AE31, post-processing corrections were applied to account for artifacts arising from both multiple scattering within the quartz fiber filter matrix and the filter-loading effect. In this study, a C_{ref} of 3.13 was uniformly applied across all wavelengths, following the methodology presented by (Luoma et al., 2021). This value was derived using the correction algorithm developed by (Arnott et al., 2005), based on comparisons with absorption measurements from a Multi-Angle Absorption Photometer (MAAP) at the same site. The *R(ATN)* was also applied to compensate for the reduction in the effective optical path length as particles accumulated on the filter. These corrections were essential for ensuring accurate σ_{abs} retrievals and for addressing known biases in AE31 measurements associated with the scattering properties of the filter substrate. The corrected data enable reliable characterization of aerosol light absorption and its spectral dependence in the boreal environment.

From January 2018 to October 2022, the AE33 aethalometer replaced the AE31 at the SMEAR II station. The AE33 incorporates a dual-spot filter design that continuously compares two filter spots with different particle loads, enabling real-time corrections for the filter-loading effect (Drinovec et al., 2015). Unlike the AE31, the AE33 does not require post-processing correction factors such as *R(ATN)*, as its dual-spot approach automatically compensates for loading effects during measurements. Additionally, the AE33 utilizes updated algorithms for

https://doi.org/10.5194/egusphere-2025-1776
Preprint. Discussion started: 13 May 2025

scattering corrections, including adjustments to C_{ref}, improving measurement accuracy under varying aerosol concentrations and environmental conditions.

The key difference between the two instruments lies in their handling of the filter-loading effect. The AE31 requires manual post-processing to address non-linear responses caused by particle accumulation, while the AE33 performs these corrections in real time, reducing the need for post-processing and enhancing data reliability. This distinction, combined with the AE33's improved algorithms, allows for more accurate and consistent measurements of aerosol properties in dynamic environments.

2.2.2 Multi-angle absorption photometer

The Thermo Scientific model 5012 multi-angle absorption photometer (MAAP) measures light absorption coefficient and equivalent black carbon concentration at a 637 nm wavelength ($\sigma_{abs,637}$ and *eBC*, respectively) with a one-minute resolution and maintains a 16.67 lmin $^{-1}$ airflow using an external pump. It collects aerosol particles on glass fiber filter tape (Saturno et al., 2017). When particle accumulation reaches a threshold, the tape advances to a new place to avoid saturation. A 637 nm light source measures transmitted photon counts at a 0° detection angle, while reflected counts are measured at 130° and 165° to assess hemispheric backscattering (Petzold et al., 2005; Petzold & Schönlinner, 2004). The aerosol layer and filter matrix are modeled as a two-layer system, using the adding method and radiation budget equations (Petzold et al., 2005; van de Hulst, 1980). These equations are solved iteratively using the single-scattering albedo of the aerosol-loaded filter layer and the layer's optical depth until convergence is achieved (Petzold & Schönlinner, 2004). The $\sigma_{abs,637}$ is then determined, from which the *eBC* concentration per unit volume is calculated. This conversion is based on a default mass absorption cross section of 6.6 m^2g^{-1}, as recommended by Petzold et al. (2005).

2.2.3 Integrating nephelometer

The TSI Incorporated model 3563 integrating nephelometer measures the light scattering and backscattering coefficients (σ_{sca} and σ_{bsca}, respectively) of the aerosol particles in their airborne state (Anderson et al., 1996). The instrument comprises three primary elements: a measurement chamber, a light source, and a detector. A diffuser guarantees that the light source emits a wavefront resembling a Lambertian distribution into the chamber. The chamber has a detector at one end and a light trap at the other. The chamber's interior is covered with black flocked paper to absorb stray light. The reference chopper positioned in front of the detector consists of three distinct sections: a signal section responsible for integrating light scattering within the range of 7° to 170°, a dark portion used to measure background noise, and a calibration section utilized to ensure the stability of the light source. A correction to address the scattering in blind angles (< 7° and > 170°) is applied according to Anderson and Ogren (1998).

A revolving backscatter shutter obstructs light within a scattering angle range of 7-90°, allowing for the measurement of hemispheric backscattering between 90° and 170°. The detector consists of three photomultiplier tubes and a lens that aligns dispersed light into parallel rays, dividing it into wavelengths of 450, 550, and 700 nm using dichroic and bandpass filters. The σ_{sca} and σ_{bsca} are determined by integrating the simplified scattering phase function. The data are corrected for gas molecule scattering by employing a HEPA filter. Regular span checks using CO_2 gas are conducted to account for instrument drift (Anderson et al., 1996).

https://doi.org/10.5194/egusphere-2025-1776
Preprint. Discussion started: 13 May 2025

2.2.4 Cascade impactor with subsequent gravimetric analysis

The sampling of ambient aerosol particles at SMEAR II has been conducted since the late 1990s using a Dekati PM_{10} cascade impactor filter with an unheated inlet for total suspended particulates (Laakso et al., 2003; Petäjä et al., 2025). The inlet, vertically sampling from approximately 5 m above ground level, consists of a stainless-steel tube with a rain cover. The impactor separates particles into three size fractions with aerodynamic diameter cut points at 10 µm (PM_{10}), 2.5 µm ($PM_{2.5}$), and 1 µm (PM_1) across its three stages. This separation is achieved with a consistent volumetric air flow rate of 30 l min^{-1} (Berner & Luerzer, 1980).

Collection substrates for the first two stages include 25 mm polycarbonate membranes (Nuclepore 800 203) without perforations. In contrast, the final stage employs a 47 mm Teflon filter with a 2 µm pore size (R2P J047) from Pall Corporation. To minimize particle rebound from the collection surfaces, the membranes are coated with a thin layer of Apiezon L vacuum grease and diluted in toluene. After collection, particulate samples are weighed in gravimetric analysis.

Particulate samples are weighed to produce aerosol mass distribution in two-to-three-day averages. The mass distributions are calculated based on the differences in filter weights before and after sampling. Once weighed, the filters are stored in a freezer to preserve the samples for future chemical and physical analyses. This procedure ensures the reliable collection, quantification, and archiving of aerosol particle data for long-term studies. The PM mass data across different aerosol particle size ranges, i.e. PM_1, $PM_{10,}$ and super-PM_{10} (>PM_{10}) was merged with the hourly resampled aerosol optical property data.

2.3 Data processing of aerosol optical and PM mass-related properties

The aerosol optical data analyzed in this study cover the period from 4 October 2010 to 4 October 2022. Optical properties for the $PM_{1\text{-}10}$ aerosol particle size fraction were derived by subtracting PM_1 aerosol particle measurements from the corresponding PM_{10} aerosol particle measurements of scattering and absorption. All optical data were initially resampled to hourly averages using a +30-minute offset, resulting in timestamps centered at, for example, 00:30:00, 01:30:00, 00:02:30 and so on. This offset reflects the standard timestamp convention used by the Environmental Database for Atmospheric Studies (EBAS), maintained by the Norwegian Institute for Air Research (NILU), where hourly values are centered within their respective averaging intervals. The actual temporal resolution of each instrument is listed in Table 1.

To enable comparison with the gravimetric PM mass measurements, the optical data were subsequently averaged within each filter sampling interval, as defined by the start and end timestamps of the impactor measurements. This was achieved by identifying overlapping timestamps between the optical and gravimetric datasets and computing the mean of the optical variables within each sampling window. The corresponding PM mass and metadata from the filter dataset were assigned to the same time windows in the optical dataset. This procedure yielded a set of time-aligned values, hereafter referred to as '*pseudo-daily mean values*'. These values provided the basis for subsequent seasonal and long-term analyses across optical and mass-based variables.

https://doi.org/10.5194/egusphere-2025-1776
Preprint. Discussion started: 13 May 2025

Hourly optical data were converted to pseudo-daily means primarily because pollen events were classified based on filter samples collected every two to three days. In contrast, the specific days on which dust events occurred were identified using the event classification presented by (Varga et al., 2023). The use of pseudo-daily resolution ensures consistency between the time bases of the optical and mass measurements, particularly for the episodic analysis. For this reason, all optical data were first resampled to the hourly timescale to facilitate precise temporal alignment and averaging across the datasets before aggregation into analysis-ready values.

Table 1. Temporal resolutions and size cut-offs of the different aerosol optical instruments

Instrument	**Temporal resolution**	**Size cut-off**
Aethalometer (AE33)	2 minutes	PM_1, PM_{10}
Multi angle absorption photometer (MAAP; Thermo Scientific model 5012)	1 minute	PM_1, PM_{10}
Integrating nephelometer (TSI Incorporated model 3563)	1 minute	PM_1, PM_{10}
Dekati Gravimetric Cascade Impactor (GCI)	2-3 days	$\leq PM_1$, $\leq PM_1$-$PM_{2.5}$, $\leq PM_{2.5}$-PM_{10}, $\leq PM_{10}$, $> PM_{10}$

In this study, we analyzed absorption data for both PM_1 and PM_{10} aerosol particles. Specifically, we utilized the MAAP data to plot $\sigma_{abs,637}$, and the AE31/33 data to plot $\sigma_{abs,660}$. Subsequently, a scatterplot was created with the MAAP data to plot $\sigma_{abs,637}$ on the x-axis and the AE31/33 data to plot $\sigma_{abs,660}$ on the y-axis. This allowed us to determine the slope and y-intercept, which were then used to scale $\sigma_{abs,660}$ data from the AE31/33 instruments to match $\sigma_{abs,637}$ from the MAAP instruments. The same correction factors (slope = 2.36 and y-intercept = -0.08; Figure S9) derived from this analysis were extended to scale the σ_{abs} data from the AE31/33 instrument at the other six wavelengths of 370, 470, 520, 550, 880 and 950 nm to correct all the data from the AE31/33 instruments.

For calculating the trends in the different aerosol optical data, the Mann-Kendall regression was used to effectively handle outliers without assuming a normal distribution (Collaud Coen et al., 2020). This method also minimizes the risk of Type I errors, which can occur when a trend is incorrectly identified as *'statistically significant'* due to an anomaly in the data (i.e., autocorrelation). Additionally, Sen-Theil's slope estimator has been used to quantify the slope of the trends, providing a reliable measure of the long-term changes in the aerosol optical properties, even if there are non-linear trends and seasonal fluctuations in the data (Collaud Coen et al., 2020).

Equation (1) was used to calculate the relative slope:

$$\text{Relative slope } (\%\text{yr}^{-1}) = \left(\frac{\text{Sen-Theil's slope}}{\text{Median of aerosol optical data}} \times 365.25\text{yr}^{-1} \times 100\%\right), \quad (1)$$

https://doi.org/10.5194/egusphere-2025-1776
Preprint. Discussion started: 13 May 2025

Two key parameters used to characterize the wavelength dependence of aerosol optical properties (AOPs) are the Absorption Ångström Exponent (AAE) and the Scattering Ångström Exponent (SAE). These exponents provide insights into aerosol composition and particle size distributions, offering indirect information about the types of aerosols present. While they are not directly used to estimate climate effects, they are important for understanding the physical and chemical properties of aerosols, which influence their behavior and interactions with radiation. Two key parameters that are routinely used to characterize the wavelength dependence of AOPs are the Ångström exponents: the *AAE* and the *SAE*.

2.3.1 Absorption Ångström exponent (*AAE*)

The *AAE* represents the wavelength dependence of aerosol light absorption and provides insights into the chemical characteristics of aerosol particles, such as brown carbon (BrC) or presence of coatings on a BC core, which have important implications for radiative forcing (Cazorla et al., 2013). The AAE was calculated by determining the slope of the ordinary least squares (OLS) linear fit of the natural logarithmic values of the σ_{abs} as a function of wavelength:

$$AAE = -\frac{\Delta \ln(\sigma_{abs,\lambda})}{\Delta \ln(\lambda)}, \quad (2)$$

where σ_{abs} represents the light absorption coefficient at wavelength λ. For AAE, absorption measurements are taken at the following 7 wavelengths: 370, 470, 520, 590, 660, 880, and 950 nm.

2.3.2 Scattering Ångström exponent (*SAE*)

The *SAE* quantifies the wavelength dependence of aerosol light scattering and is closely associated with aerosol particle size distribution. Higher *SAE* values generally indicate a dominance of smaller, fine-mode particles, which exhibit a stronger wavelength dependence in scattering behavior. Conversely, lower *SAE* values are associated with larger, coarse-mode particles that scatter light more uniformly across wavelengths. This relationship makes the *SAE* a valuable metric for assessing aerosol size distributions, providing insight into the relative abundance of fine and coarse particles and their implications for atmospheric radiative properties and climate-forcing (Schuster et al., 2006).

In this study, the *SAE* was calculated similarly to the *AAE* by applying an Ordinary Least Squares (OLS) linear regression to the natural logarithmic values of the light scattering coefficients at 450, 550, and 700 nm, regressed against the natural logarithmic values of these wavelengths, as shown in Equation 3:

$$SAE = -\frac{\Delta \ln(\sigma_{sca,\lambda})}{\Delta \ln(\lambda)}, \quad (3)$$

2.3.3 Single scattering albedo (*SSA*)

The *SSA* is a key aerosol optical property that is defined as the ratio of the σ_{sca} to the total extinction coefficient (the sum of σ_{sca} and σ_{abs}). The *SSA* is instrumental in determining whether aerosols exert a net cooling or warming effect on the atmosphere: higher *SSA* values generally indicate that aerosols are primarily scattering, contributing to a cooling effect, while lower *SSA* values suggest a more significant role in absorption, which leads to warming

https://doi.org/10.5194/egusphere-2025-1776
Preprint. Discussion started: 13 May 2025

(Bond et al., 2013; Luoma et al., 2019; Tian et al., 2023). *SSA* can be calculated at any wavelength; in this study, *SSA* was calculated explicitly at 550 nm (hereon SSA_{550}).

2.3.4 Mass absorption coefficient (*MAC*)

The *MAC* represents the efficiency with which aerosol particles absorb light per unit mass (not to be confused with *MAC* of BC, which is used in convertion of σ_{abs} to BC). The *MAC* is sensitive to changes in aerosol chemical composition and is a valuable indicator of shifts in absorbing components, such as BC and certain light absorbing organic compounds (i.e., BrC). These changes in the *MAC* often reflect variations in aerosol sources or chemical aging processes (Andreae & Gelencsér, 2006; Bond & Bergstrom, 2006). Long-term studies on *MAC* can reveal trends in aerosol composition, especially in regions like the Arctic and boreal environments, where variations in pollution sources and climate-driven changes are prevalent.

2.3.5 Mass scattering coefficient (*MSC*)

The *MSC* quantifies the efficiency with which aerosol particles scatter light per unit mass. In contrast to the *MAC*, the *MSC* is primarily influenced by the physical characteristics of aerosols—especially particle size, shape, and composition—as these properties impact light-scattering efficiency per unit mass (Bates et al., 2005; Seinfeld & Pandis, 2016). Higher *MSC* values are typically associated with a more significant proportion of scattering particles, such as sulfate, nitrate, and other non-absorbing components, which contribute to a cooling effect in the planetary boundary layer (PBL), partially counteracting the warming effect of absorbing aerosols (Pandolfi et al., 2014).

3. Results and discussion

3.1 General characteristics of $PM_{1–10}$ aerosol particles

Long-term observations at SMEAR II indicate that $PM_{1–10}$ primarily contributes to aerosol scattering, with minimal absorption due to its composition, which is predominantly influenced by aerosol particles of biogenic origin (e.g., pollen, fungal spores) and mineral dust (Luoma et al., 2019; Zieger et al., 2015). The *SSA* remains consistently high (>0.90), while the *MSC* is lower than that of PM_1, aligning with Mie theory predictions for larger particles (Pandolfi et al., 2018; Titos et al., 2021). A summary of these descriptive statistics for PM1–10 aerosol particles is provided in Table 2. Seasonal variations reveal increased $PM_{1–10}$ scattering during spring and early summer due to enhanced biogenic activity, particularly from pollen and fungal spores (Heikkinen et al., 2020; Yli-Panula et al., 2009), whereas winter conditions favor fine-mode aerosols, reducing the relative contribution of $PM_{1–10}$ (Luoma et al., 2021).

Intermittent mineral dust intrusions, predominantly from the Aral-Caspian region, contribute to episodic increases in atmospheric dust concentrations over Finland (Varga et al., 2023). While these events introduce coarse-mode aerosols, their influence on the absorption properties of $PM_{1–10}$, particularly in terms of MAC variability, remains poorly characterized due to limited long-term observations and uncertainties in aerosol source contributions. Lihavainen et al. (2015) analyzed long-term aerosol optical properties at the Pallas Global Atmospheric Watch

https://doi.org/10.5194/egusphere-2025-1776
Preprint. Discussion started: 13 May 2025

station, focusing on PM_{10} rather than specifically $PM_{1–10}$, but their findings on seasonal variations in scattering and absorption provide useful context for interpreting boreal aerosol trends.

Hygroscopic growth measurements suggest that $PM_{1–10}$ is less effective as cloud condensation nuclei (CCN) compared to fine-mode aerosols, influencing its atmospheric lifetime and radiative effects (McFiggans et al., 2006). While Lihavainen et al. (2015) examined aerosol hygroscopic properties in northern Finland, their study primarily covered PM_{10} rather than isolating the $PM_{1–10}$ fraction. The contribution of $PM_{1–10}$ to total PM_{10} scattering at SMEAR II remains substantial, though its representation in optical measurements is uncertain due to limitations in nephelometry and aethalometry, which tend to underestimate coarse-mode aerosol properties (Brasseur et al., 2024; Zieger et al., 2015).

Table 2. Descriptive statistics of the aerosol optical properties for all the valid data of the PM_{1-10} particles.

		Wavelength (nm)	$PM_{1–10}$ aerosol particles				
Extensive variables			25%ile	Mean	Median	75%ile	Std. dev.
	σ_{abs} (Mm^{-1})	520	0.09	0.18	0.14	0.22	0.16
	σ_{sca} (Mm^{-1})	550	1.75	3.35	2.75	4.19	2.55
	PM mass (μgm^{-3})		0.97	2.33	1.58	2.55	3.51
Intensive variables	*AAE* (dimensionless)	370-950	0.57	0.73	0.74	0.89	0.33
	SAE (dimensionless)	450-700	0.11	0.24	0.32	0.58	0.81
	SSA (dimensionless)	550	0.93	0.94	0.95	0.96	0.04
	MAC (m^2g^{-1})	520	0.05	0.11	0.08	0.14	0.86
	MSC (m^2g^{-1})	550	1.07	1.92	1.61	2.65	11.64

3.2 Long-term trends of extensive properties

Extensive properties refer to the properties of aerosol particles that depend on the amount of the aerosol particles. From the studied extensive properties, $\sigma_{sca,550}$, $\sigma_{abs,520}$ and mass for $PM_{1–10}$ aerosol particles show a clear long-term negative trend from October 2010 to October 2022, reflecting a decline in optical and mass properties (Figure. 1). To compare the relative differences with $PM_{1–10}$, trends for PM_1 and PM_{10} size fractions are also studied, and all the trends are presented in Table 3.

This decrease aligns with earlier findings at SMEAR II, as reported by Luoma et al. (2019), where reductions in extensive properties were attributed to declines in particle number concentration and volume concentrations, particularly impacting larger accumulation mode and coarse-mode aerosol particles with peaks at approximately 700 nm and 5 µm, respectively.

Pollen and dust events, marked as green and red stars in all figures where they are plotted, contribute additional variability to the observed optical and mass properties. Pollen events are typically seasonal, occurring during spring and summer, and contribute significantly to particle mass and scattering in the $PM_{1–10}$ size range. Dust events, which are more intermittent and often result from long-range transport, enhance scattering and mass

https://doi.org/10.5194/egusphere-2025-1776
Preprint. Discussion started: 13 May 2025

concentrations in the coarse mode, including $PM_{1–10}$ aerosol particles. While these events introduce short-term variability, they do not alter the overall long-term declining trends. The pseudo-daily mean values used in this analysis help to better highlight such events by providing a finer temporal resolution, enabling the identification of short-term peaks in optical and mass properties alongside the broader trends.

Table 3. Long-term trends and statistical significance of $PM_{1–10}$ aerosol optical and PM_{1-10} mass properties.

S. No.	Variable	Slope	Relative trend	p-value	Statistical significance
(a)	$\sigma_{sca,\,550}$ (Mm^{-1})	$1.05 \times 10^{-2} \pm 0.05$ $Mm^{-1}yr^{-1}$	0.39 ± 1.67 $\%yr^{-1}$	0.71	No
(b)	$\sigma_{abs,\,520}$ (Mm^{-1})	$-9.57 \times 10^{-3} \pm 2.46 \times 10^{-3}$ $Mm^{-1}yr^{-1}$	-7.38 ± 1.90 $\%yr^{-1}$	6.23×10^{-11}	Yes
(c)	*SAE* (dimensionless)	-0.05 ± 0.02 yr^{-1}	-12.83 ± 4.63 $\%yr^{-1}$	3.01×10^{-8}	Yes
(d)	*AAE* (dimensionless)	$0.03 \pm 7.86 \times 10^{-3}$ yr^{-1}	4.60 ± 1.09 $\%yr^{-1}$	6.73×10^{-13}	Yes
(e)	*PM mass* (μgm^{-3})	-0.04 ± 0.04 $\mu gm^{-3}yr^{-1}$	-2.94 ± 2.43 $\%yr^{-1}$	0.02	Yes
(f)	SSA_{550} (dimensionless)	$2.63 \times 10^{-3} \pm 8.88 \times 10^{-4}$ yr^{-1}	0.28 ± 0.09 $\%yr^{-1}$	1.31×10^{-7}	Yes
(g)	MSC_{550} (m^2g^{-1})	$6.43 \times 10^{-3} \pm 1.07 \times 10^{-2}$ $m^2g^{-1}yr^{-1}$	0.39 ± 0.66 $\%yr^{-1}$	0.22	No
(h)	MAC_{520} (m^2g^{-1})	$-2.66 \times 10^{-3} \pm 6.69 \times 10^{-4}$ $m^2g^{-1}yr^{-1}$	-3.47 ± 0.87 $\%yr^{-1}$	1.44×10^{-14}	Yes

https://doi.org/10.5194/egusphere-2025-1776
Preprint. Discussion started: 13 May 2025

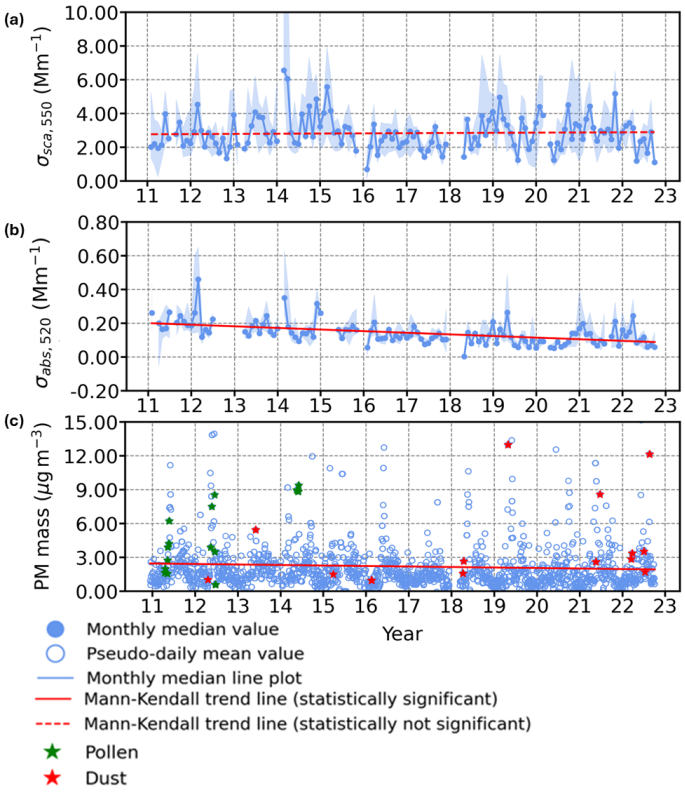

Figure 1. Time series of (a) $\sigma_{sca,550}$, (b) $\sigma_{abs,520}$ and (c) *PM mass* for the $PM_{1–10}$ size aerosol particles from October 2010 to October 2022.

3.2.1 Scattering coefficient ($\sigma_{sca,550}$)

Scattering due to PM_1 aerosol particles at SMEAR II shows a trend of −0.26 ± 0.17 Mm^{-1} yr^{-1}; −3.48 ± 2.33 % yr^{-1} (Figure S2(a); Table S4(a)). Submicron particles dominate aerosol light scattering at the site (Virkkula et al., 2011), suggesting that $\sigma_{sca,550}$ is influenced primarily by fine-mode aerosol loading. The observed negative trend is consistent with reductions in anthropogenic sulfur dioxide (SO_2) emissions, which contribute to secondary sulfate formation, a major component of PM_1 aerosol mass and associated optical properties (Smith et al., 2011). Regionally, similar decreases in aerosol scattering have been reported at multiple European background stations (Pandolfi et al., 2018), further supporting the possibility of a widespread decline in fine-mode aerosol scattering. SMEAR II is also subject to seasonal biogenic emissions, particularly monoterpenes that contribute to secondary organic aerosol (SOA) formation (Hakola et al., 2003; Hallquist et al., 2009; Rantala et al., 2015). However, long-term records indicate that biogenic VOC emissions at this site have remained relatively stable over the past two decades (Kulmala et al., 2001). As such, no evidence currently supports a significant contribution of BVOC variability to the observed multi-year decline in PM_1 scattering. Taken together, the trend observed at SMEAR II

https://doi.org/10.5194/egusphere-2025-1776
Preprint. Discussion started: 13 May 2025

is consistent with known reductions in anthropogenic precursor emissions, particularly SO_2, though additional factors cannot be excluded.

3.2.2 Absorption coefficient ($\sigma_{abs,\,520}$)

The absorption coefficient ($\sigma_{abs,520}$) for $PM_{1–10}$ shows a statistically significant decrease, with a trend of -9.57 × 10^{-3} ± 2.46 × 10^{-3} $Mm^{-1}yr^{-1}$; 7.38 ± 1.90 $\%yr^{-1}$ (Figure 1(b); Table 3(b)). This slower decline compared to smaller particles highlights the lower sensitivity of $PM_{1–10}$ to reductions in absorbing materials. By contrast, $\sigma_{abs,520}$ of the PM_{10} aerosol particles decline at -0.11 ± 0.03 $Mm^{-1}yr^{-1}$; -8.18 ± 1.94 $\%yr^{-1}$ (Figure S1(b); Table S3(b)) and of the PM_1 aerosol particles decline (-0.10 ± 0.02 $Mm^{-1}yr^{-1}$; -8.38 ± 2.03 $\%yr^{-1}$) (Figure S2(b); Table S4(b)). These differences emphasize the limited role of absorption in $PM_{1–10}$, likely due to its composition and the dominance of coarse-mode aerosols such as mineral dust, pollen, and fungal spores, which scatter light more efficiently than they absorb it (Laskin et al., 2005; Moosmüller et al., 2009).

The weaker absorption trend in $PM_{1–10}$ suggests that reductions in absorbing aerosols, such as BC and BrC, have had a more pronounced effect on fine-mode particles. Coarse-mode absorption is typically associated with mineral dust and biological aerosols rather than combustion-related emissions, which dominate absorption in finer particles. While super-PM_{10} particles (>10 µm) share similar scattering properties, their influence on absorption trends remains less certain due to their shorter atmospheric residence time and more efficient removal via gravitational settling (Emerson et al., 2020; Zhang et al., 2001). The role of instrumental differences, despite calibration with MAAP, should also be considered when interpreting these trends, as sensitivity variations between instruments may affect long-term trend analyses (Collaud Coen et al., 2010).

3.2.3 PM mass concentration

Although this study focuses on PM_1 and PM_{1-10} fractions, investigating trends in super-PM_{10} aerosols may provide additional insights into long-term shifts in coarse-mode aerosol composition that are not detected by the optical instruments and the used 10 µm cut-off. Super-PM_{10} particles, which include biological aerosols (e.g., pollen, fungal spores) and mineral dust, are strongly influenced by episodic events such as seasonally driven biological emissions and long-range dust transport. However, their long-term trends remain poorly constrained.

The variability in super-PM_{10} aerosols likely reflects a combination of natural and anthropogenic influences. While mineral dust and pollen contribute significantly to coarse-mode particles, their variability is largely seasonal and event-driven. In contrast, fine-mode particles (PM_1) and PM_{1-10} aerosols exhibit more consistent long-term trends due to anthropogenic emissions. The decline in PM_1 mass concentrations aligns with reductions in both primary and secondary anthropogenic aerosol sources. However, PM_{1-10} contains a larger fraction of natural aerosols, which exhibit substantial variability but may not necessarily follow a long-term trend.

Previous studies (Leskinen et al., 2012; Varga et al., 2023) have highlighted the episodic nature of coarse-mode aerosol contributions, including periods of increased dust transport to Finland, particularly after 2010 (Varga et al., 2023). The frequency of these events, combined with changes in regional meteorology and source contributions, may introduce variability in observed PM_{1-10} trends. In this study, we further assess the relative

https://doi.org/10.5194/egusphere-2025-1776
Preprint. Discussion started: 13 May 2025

contributions of biological aerosols and mineral dust by comparing super-PM_{10} variations with $PM_{1\text{-}10}$, providing insights into their role in long-term aerosol trends and atmospheric transport patterns.

3.3 Long-term trends of intensive properties

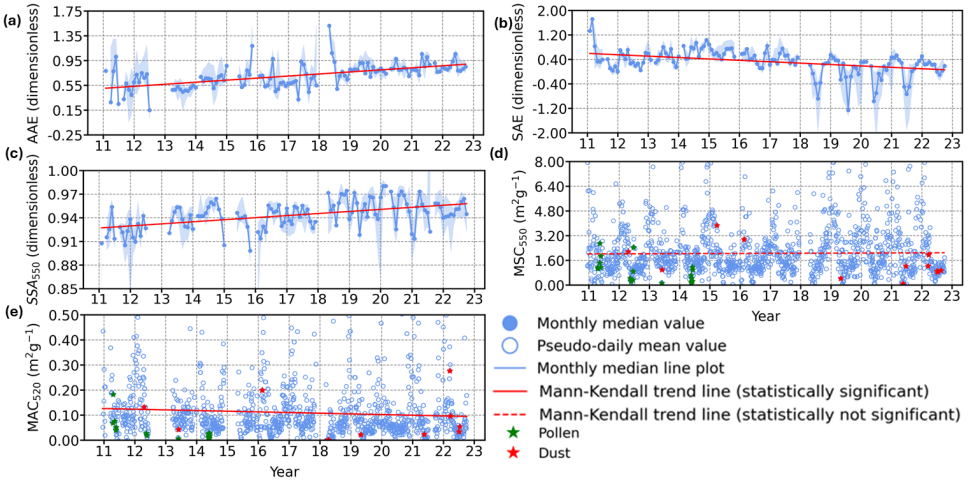

Figure 2. Time series of (a) *AAE*, (b) *SAE*, (c) SSA_{550}, (d) MSC_{550} and (e) MAC_{520} for the PM_{1-10} aerosol particles from October 2010 to October 2022.

3.3.1 Absorption Ångström exponent (*AAE*)

The *AAE* for PM_{1-10} aerosol particles exhibits a statistically significant decreasing trend with a slope of 0.03 ± 7.86×10^{-3} yr^{-1}; 4.60 ± 1.09 $\%yr^{-1}$ (Figure 2(a); Table 3(d)), suggesting a shift in aerosol composition. PM_{10} aerosol particles also display a negative trend of $-1.13 \times 10^{-2} \pm 5.03 \times 10^{-3}$ yr^{-1}; -1.01 ± 0.45 $\%yr^{-1}$ (Figure S3(a); Table S3(d)), while PM_1 aerosol particles exhibit a smaller but still decreasing trend of $-1.37 \times 10^{-2} \pm 6.29 \times 10^{-3}$ yr^{-1}, -1.16 ± 0.54 $\%yr^{-1}$ (Figure S4(a); Table S4(d)), which could be attributed to the dominance of BC in the fine aerosol particle fraction. The more pronounced decrease in PM_{1-10} suggests a potential decline in BrC, possibly due to enhanced oxidation processes or a shift toward less absorbing organic aerosols. This aligns with long-term reductions in BC concentrations at Hyytiälä (Luoma et al., 2021) and shifts in organic aerosol sources (Äijälä et al., 2019; Heikkinen et al., 2020). Given that BC is predominantly submicron, the decreasing *AAE* in PM_{1-10} is more likely to reflect changes in BrC absorption characteristics in the coarse-mode fraction rather than BC variability alone.

A notable abrupt change in *AAE* values is observed between pre-2018 and post-2018, which may be linked to the instrumental transition from AE31 to AE33 in March 2018. The AE33 Aethalometer introduces real-time filter-loading corrections through a dual-spot measurement approach, which effectively reduces filter-loading biases inherent to the AE31 model (Drinovec et al., 2015). This methodological difference has been shown to impact BC and BrC estimates, particularly influencing *AAE* calculations (Backman et al., 2017; Zotter et al., 2017). Also, Luoma et al. (2021) showed how *AAE* varies between different aethalometer correction algorithms. Interestingly,

https://doi.org/10.5194/egusphere-2025-1776
Preprint. Discussion started: 13 May 2025

this discontinuity is not observed in PM_1 or PM_{10} *AAE* trends, which suggests that the AE31-to-AE33 transition might have introduced size-dependent effects in *AAE* calculations. Previous studies indicate that AE33 generally yields lower *AAE* values than AE31, especially at shorter wavelengths where BrC absorption dominates, which could affect how BrC in coarse-mode aerosols ($PM_{1–10}$) is quantified (Bernardoni et al., 2021; Zotter et al., 2017).

While these differences align with known AE31-to-AE33 biases, further analysis is needed to determine whether the observed *AAE* shift stems solely from instrumental changes or also reflects atmospheric variations. Examining the *AAE* wavelength dependence across size fractions and assessing potential modifications in BrC optical properties could help separate instrumental artifacts from real aerosol composition trends. At least one previous study, Bali et al. (2024), highlights the importance of BrC optical properties in interpreting long-term aerosol trends, particularly in environments influenced by SOA and episodic biomass-burning events.

3.3.2 Scattering Ångström exponent (*SAE*)

The *SAE* for PM_{1-10} particles exhibits a negative trend of -0.05 ± 0.02 yr^{-1}; -12.83 %yr^{-1} (Figure 2(b); Table 3(c)), indicating a declining influence of smaller particles (closer to 1 µm) or a slower decline of larger particles (closer to 10 µm), given concurrent decreases in $\sigma_{sca,550}$ and *PM mass*. This suggests that fine-mode aerosols within PM_{1-10} are decreasing at a faster rate than those in the 2.5–10 µm range, leading to a relative dominance of larger particles rather than an absolute increase. The observed trend may be driven by reduced secondary aerosol formation or changes in atmospheric processing (Maso et al., 2005; Seinfeld & Pandis, 2016). A decline in fine-mode SOA condensation onto pre-existing particles could limit fine-mode growth, shifting the relative contribution of supermicron particles (>1 µm). Additionally, long-term reductions in sulfate emissions make it unlikely that an increase in sulfate mass is responsible for the shift in *SAE*. Instead, changes in dust concentrations could play a role, although long-term dust trends remain uncertain. The negative *SAE* trend observed for PM_{10} (Figure S3.b) further suggests a greater relative contribution of larger particles within PM_{10}, likely due to a slower decline in the 2.5–10 µm range compared to fine-mode particles (1–2.5 µm). Aerosol particles in this size range, including mineral dust, sea salt, pollen, and fungal spores, exhibit different atmospheric lifetimes and removal processes than finer particles, contributing to differences in observed trends.

For PM_1 (Figure S4(b)), *SAE* remains stable, suggesting no major shifts in fine-mode size distributions. This stability indicates that the ratio of BC to scattering components, primarily sulfate and organics, has not changed significantly over time. Luoma et al. (2019) reported a decrease in volume mean diameter (VMD) from ~0.25 µm to ~0.2 µm (2006–2017), indicating a long-term shift toward smaller aerosol sizes. While this period does not fully overlap with this study, the trend likely continued, though more recent data would be needed to confirm this assumption. The observed differences between PM_1 and PM_{1-10} *SAE* trends highlight the distinct processes influencing fine and larger aerosols, including atmospheric processing, long-range transport, and primary emissions. Reduced SOA condensation onto fine particles may further enhance the relative contribution of larger particles in PM_{10}. However, while pollen (>10 µm) is classified as a coarse aerosol in this study, its influence on SAE trends is likely minimal, as infrequent high concentrations from pollen events are statistically down-weighted in the calculation of monthly medians. The concurrent decline in $\sigma_{sca,550}$ and *PM mass* indicates that the negative *SAE* trend is not due to an absolute increase in large particles but rather a differential reduction in size fractions.

https://doi.org/10.5194/egusphere-2025-1776
Preprint. Discussion started: 13 May 2025

Together, these findings suggest that ongoing changes in secondary aerosol formation and primary emissions are influencing the evolution of aerosol size distributions in different size fractions.

3.3.3 Single scattering albedo (SSA_{550})

The SSA_{550} for $PM_{1\text{-}10}$ particles exhibits a small positive trend with a slope of $2.63 \times 10^{-3} \pm 8.88 \times 10^{-4}$ yr^{-1}; 0.28 ± 0.09 $\%yr^{-1}$ (Figure 2(c); Table 3(f)), indicating an increase in scattering relative to absorption. This trend has been attributed to reductions in BC contributions or increases in non-absorbing components such as sulfates and organic matter (Bond et al., 2013; Luoma et al., 2019; Pandolfi et al., 2014). However, these references provide general evidence on aerosol composition rather than site-specific confirmation for Hyytiälä. Given the decline in SO_2 emissions over recent decades, a significant increase in sulfate in the coarse fraction appears unlikely. Instead, an enhanced contribution from mineral dust, a known scattering agent, could provide a more plausible explanation. However, trends in dust concentrations at the site remain uncertain due to a lack of direct long-term observations. A similar increasing SSA_{550} trend is observed for PM_{10} particles (Figure S3(c)), reinforcing the hypothesis that larger particles within PM_{10} are playing a greater role in scattering. In contrast, SSA_{550} for PM_1 particles (Figure S4(c)) remains stable, suggesting no significant long-term shift in the relative proportions of absorbing and scattering aerosols in the fine mode. This stability does not necessarily indicate the dominance of strongly absorbing BC but rather suggests that the ratio of BC to scattering components, primarily sulfate and organics, has not changed significantly over time.

Long-term chemical composition measurements at Hyytiälä provide additional insight into these trends. Heikkinen et al. (2021) and Äijälä et al. (2019) reported that organic aerosol remains the dominant fraction, but its variations have been largely seasonal rather than indicative of a sustained long-term increase. OA consists of both primary organic aerosol (POA), which is directly emitted from sources such as biomass burning and fossil fuel combustion, and SOA, which forms through gas-phase oxidation of volatile organic compounds (VOCs). While these studies discuss OA in the context of its chemical composition and seasonal variations, they do not explicitly distinguish between POA and SOA when assessing long-term trends. Additionally, ammonium sulfate, a key scattering component, has not shown an increasing trend in the coarse fraction that would explain the observed *SSA* rise in $PM_{1\text{-}10}$ and PM_{10}. The increase in SSA_{550} in these size fractions may instead be influenced by changes in dust concentrations or primary aerosol sources, though direct evidence for these trends at Hyytiälä is lacking. While mineral dust is a plausible explanation for the increase in SSA_{550}, long-term regional data on dust concentrations are needed to confirm this hypothesis. The observed stability of SSA_{550} in PM_1 particles further suggests that the balance between absorbing and scattering components in the fine mode has remained relatively unchanged. This indicates that while SSA_{550} trends in $PM_{1\text{-}10}$ and PM_{10} may be influenced by shifts in scattering aerosol composition, the fine mode remains relatively stable in its overall composition.

3.3.4 Mass scattering coefficient (MSC_{550})

The MSC_{550} represents the scattering efficiency of aerosol particles per unit mass and is a key parameter in assessing their radiative effects. The PM_{10} aerosol particles exhibit an upward trend, albeit statistically significant, with a slope of $0.04 \pm 1.19 \times 10^{-2}$ $m^2g^{-1}yr^{-1}$; 1.65 ± 0.45 $\%yr^{-1}$ (Figure S3(d); Table S3(g)), reinforcing the role of

https://doi.org/10.5194/egusphere-2025-1776
Preprint. Discussion started: 13 May 2025

scattering aerosols across different size fractions. The observed changes may be linked to long-term reductions in anthropogenic emissions and variations in aerosol sources, which influence particle composition and optical properties (Ehn et al., 2014; Pandolfi et al., 2014). Additionally, shifts in aerosol size distribution could contribute to the increasing MSC_{550} trend for the PM_{10} aerosol particles, as larger particles scatter light less efficiently per unit mass compared to the PM_1 aerosol particles.

Even the PM_1 aerosol particles exhibits a similarly increasing trend in MSC_{550}, with a trend of $0.05 \pm 1.21 \times 10^{-2}$ $m^2g^{-1}yr^{-1}$; -1.46 ± 0.37 $\%yr^{-1}$ (Figure S4(d); Table S4(g)). This increase indicates that fine-mode aerosol particles, which are primarily composed of secondary organic aerosols and sulfates, have experienced a more or less similar trend in their scattering efficiency per unit mass. This trend may reflect changes in precursor emissions, aerosol aging processes, or chemical transformations in the atmosphere. Additionally, reductions in sulfate mass fractions within PM_1 could lead to a lower MSC_{550}, as sulfates are highly efficient scatterers (Pandolfi et al., 2014; Seinfeld & Pandis, 2016). Given the importance of scattering aerosols in modulating radiative forcing, long-term observations of MSC_{550} remain essential for understanding aerosol–radiation interactions and improving climate model predictions.

3.3.5 Mass absorption coefficient (MAC_{520})

The MAC_{520} for $PM_{1\text{-}10}$ aerosol particles exhibits a statistically significant decreasing trend, with a slope of $-2.66 \times 10^{-3} \pm 6.69 \times 10^{-4}$ $m^2g^{-1}yr^{-1}$; -3.47 ± 0.87 $\%yr^{-1}$ (Figure 2(e); Table 3(h)). This decline suggests a reduction in the light-absorbing efficiency per unit mass, likely driven by decreasing BC contributions or chemical transformations in absorbing aerosol particles (Bergstrom et al., 2007; Lack & Cappa, 2010). The decreasing trend is consistent with long-term reductions in anthropogenic emissions, although the observed MAC_{520} trend in the $PM_{1\text{-}10}$ fraction raises questions regarding its underlying causes. While the MAC_{520} is defined for all aerosol size fractions, its variability in $PM_{1\text{-}10}$ aerosol particles is influenced by both the presence of black carbon (BC) and the potential effects of measurement uncertainties. This raises the possibility that either (1) BC-containing particles contribute to the MAC_{520} in the coarse mode or (2) measurement artifacts are affecting the trend. A similar decreasing trend in PM_{10} (Figure S3(e)) suggests that changes in absorbing components are affecting multiple size fractions, while the weaker trend in PM_1 (Figure S4(e)) aligns with the persistence of BC in finer aerosols.

A potential contributing factor to this trend is the transition from Aethalometer AE31 to AE33 in March 2018. This instrument change may have introduced a discontinuity in the MAC_{520} values due to differences in filter-loading correction and multiple-scattering adjustments (Drinovec et al., 2015). Unlike AE31, which requires post-processing corrections, AE33 applies a real-time dual-spot correction method, known to yield systematically lower absorption values (Zotter et al., 2017). This suggests that part of the observed decline in the MAC_{520} may be attributed to instrument-related biases rather than actual atmospheric changes.

3.4 Seasonal variability of the extensive properties

The $\sigma_{abs,520}$ follows a strong seasonal cycle, with the highest values observed in winter (December, January and February) due to increased BC emissions from residential wood burning (Kukkonen et al., 2020; Pandolfi et al.,

https://doi.org/10.5194/egusphere-2025-1776
Preprint. Discussion started: 13 May 2025

2014) in Finland. Additionally, the lower PBL during winter reduces vertical dispersion, leading to higher near-surface aerosol concentrations due to thermal inversion (Petäjä et al., 2016). These findings are consistent with Hyvärinen et al. (2011), which reported elevated BC concentrations in Finland during winter, primarily due to increased heating emissions and stable atmospheric conditions. In contrast, $\sigma_{abs,520}$ values are lower in May, June and July, mainly due to reduced heating emissions and an elevated PBL, which enhances aerosol dispersion (Arola et al., 2011). It is also possible that the correction algorithms were not entirely sufficient to minimize the sensitivity of the absorption measurements to the accumulation of aerosol particles on the filter. Meanwhile, the $\sigma_{sca,550}$ for PM_{10}, PM_1, and PM_{1-10} also exhibits distinct seasonal variability, with the highest values occurring in summer (June, July and August) and the lowest in April and October (Figures S5.a, S6.a, and 3.a). The summer peak is attributed to increased emissions of BVOCs and enhanced SOA formation, consistent with findings that SOA dominates aerosol composition in boreal regions during summer (Kourtchev et al., 2016; Tunved et al., 2006).

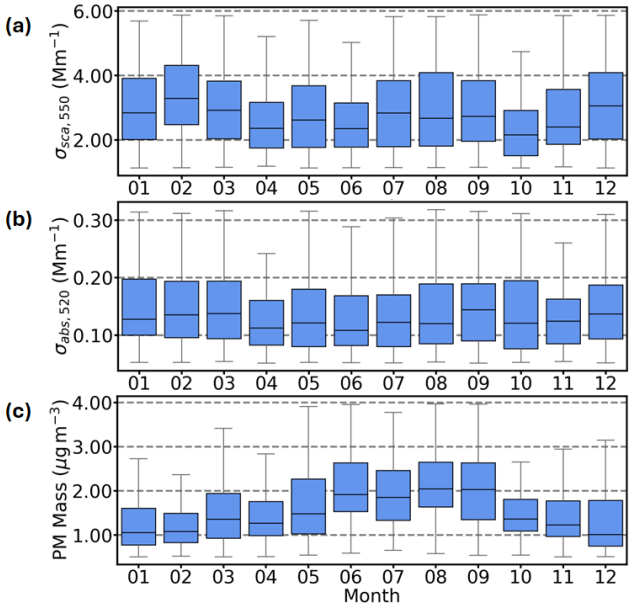

Figure 3. Monthly variations of aerosol optical properties for the PM_{1-10} aerosol particles from October 2010 to October 2022 (a) $\sigma_{sca,550}$, (b) $\sigma_{abs,520}$, and (c) PM mass. Box plots represent the interquartile range, with the first horizontal line showing the 25th percentile, the middle line showing the median (50th percentile), and the third horizontal line showing the 75th percentile. Whiskers extend to the 10th and 90th percentiles.

The April and October minima are linked to reduced household heating emissions in spring and their delayed onset in autumn, along with weaker long-range transport contributions during these transitional months (Hienola et al., 2013). The seasonal variation in PM mass at Hyytiälä, as shown in Figure S5(c) for PM_{10}**,** Figure S6(c) for PM_1 and Figure 3(c) for PM_{1-10} aerosol particles, further highlights differences between aerosol size fractions. PM_1 mass concentrations increase significantly during June–August, coinciding with enhanced SOA production, as indicated by the concurrent rise in $\sigma_{sca,550}$ for PM_1 Figures S6(a). These trends align with long-term aerosol

https://doi.org/10.5194/egusphere-2025-1776
Preprint. Discussion started: 13 May 2025

observations in Finland (Luoma et al., 2019), which report similar seasonal variations in PM mass and composition. Meanwhile, PM_{10} and $PM_{1–10}$ mass also show seasonal variability, increasing in May, coinciding with the peak in birch pollen emissions (Yli-Panula et al., 2009). Additionally, June and July peaks in these fractions may indicate long-range transported mineral dust from the Aral-Caspian and Middle Eastern regions (Varga et al., 2023). Seasonal variations in atmospheric transport and aerosol sources further contribute to these trends, with summer months favoring photochemical activity and secondary aerosol formation, while winter remains dominated by local primary emissions.

3.5 Seasonal variability of the intensive properties

The seasonal variability of intensive aerosol properties at Hyytiälä provides insight into the sources and composition of PM_{10} and $PM_{1\text{-}10}$ aerosol particles. Figures 4(d) and 4(e) illustrate the monthly variations of the MAC_{520} and the MSC_{550}. MAC_{520} peaks in winter due to increased emissions from biomass burning and residential heating, as shown by Heikkinen et al. (2021) and Virkkula et al. (2011). Reduced boundary-layer heights further enhance BC accumulation, leading to higher MAC_{520} values. Conversely, the MAC_{520} declines in summer due to the dominance of SOA from biogenic sources (Äijälä et al., 2019). Organic aerosols scatter more light than they absorb, reducing the MAC_{520} values. The seasonal minimum in the imaginary part of the refractive index further indicates lower absorption capacity in summer, reinforcing the shift toward scattering-dominated aerosols (Virkkula et al., 2011).

The MSC_{550} follows a distinct seasonal cycle, with peak values in winter (Figure 4(d)). The prevalence of fine-mode PM_1 particles, primarily from residential heating, enhances light scattering (Hellén et al., 2008). Although BC is present, the aerosol mixture includes significant amounts of scattering species such as SOA and sulfates, leading to high MSC_{550} values (Seinfeld & Pandis, 2016). Despite an increase in the *PM mass* in summer, MSC_{550} declines due to a shift toward larger particles that scatter light less efficiently per unit mass (Tunved et al., 2006). The seasonal reduction in the MSC_{550} aligns with greater contributions from pollen, mineral dust, and sea salt aerosols in the $PM_{1\text{-}10}$ fraction, altering the aerosol size distribution (Latimer & Martin, 2019). These shifts emphasize the importance of size-dependent scattering efficiency in shaping seasonal aerosol optical properties.

https://doi.org/10.5194/egusphere-2025-1776
Preprint. Discussion started: 13 May 2025

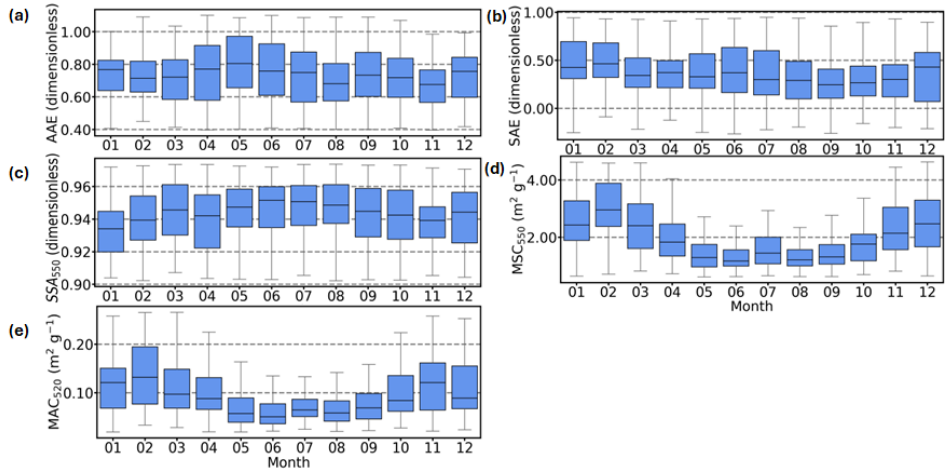

Figure 4. Monthly variations of aerosol optical properties for the PM_{1-10} aerosol particles from October 2010 to October 2022 (a) AAE, (b) SAE, (c) SSA_{550}, (d) MSC_{550} and (e) MAC_{520}. Box plots represent the interquartile range, with the first horizontal line showing the 25th percentile, the middle line showing the median (50th percentile), and the third horizontal line showing the 75th percentile. Whiskers extend to the 10th and 90th percentiles.

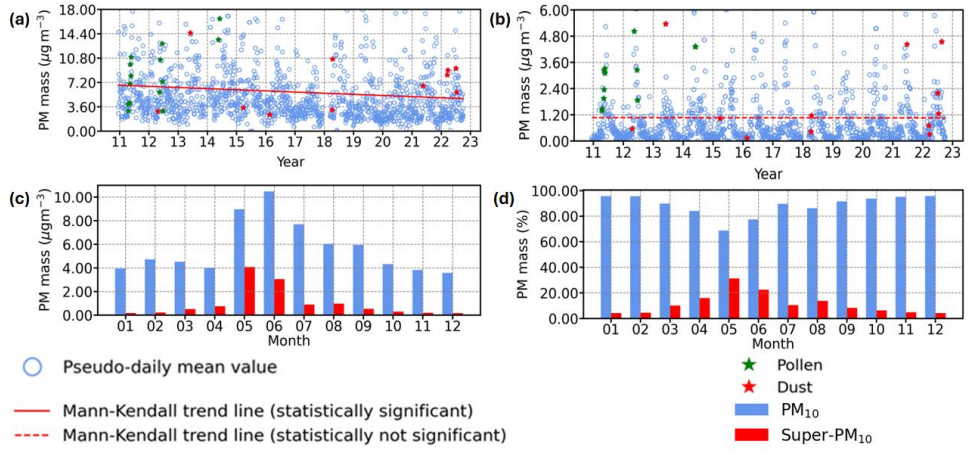

Figure 5. Temporal trend comparisons of PM mass in (a) PM_{10}, (b) super-PM_{10} aerosol particles and seasonal variation comparisons of PM_{10} and super-PM_{10} aerosol particles in terms of (c) PM mass concentration and (d) PM mass fraction.

The PM_{1-10} fraction significantly influences seasonal aerosol dynamics, particularly in spring and summer when pollen and mineral dust events contribute to coarse-mode aerosol mass. However, optical measurements in this study are constrained by the PM_{10} inlet, excluding particles larger than 10 μm. Figure 5 quantifies this missing PM fraction, showing substantial coarse-mode mass is unaccounted for, especially during episodic events. The

https://doi.org/10.5194/egusphere-2025-1776
Preprint. Discussion started: 13 May 2025

seasonal increase in PM_{1-10} and PM_{10} mass suggests coarse-mode aerosols dominate specific periods, yet their optical contributions remain uncertain. Complementary measurement techniques are needed to capture the full size distribution of coarse-mode particles and improve the representation of their optical properties. The exclusion of super-PM_{10} from optical instruments introduces uncertainties in radiative forcing assessments, underscoring the necessity of including larger particles in aerosol characterization.

Pseudo-daily peaks in super-PM_{10} mass (Figure 5) indicate that episodic events, such as pollen and dust outbreaks, significantly impact aerosol optical properties. These events contribute to short-term fluctuations in the MAC_{520} and the MSC_{550}, reflecting shifts in aerosol composition and size distribution. The variability of super-PM_{10} mass suggests coarse-mode particles play a crucial role in modifying scattering and absorption properties, further complicating aerosol–radiation interactions. Without direct optical measurements of these particles, their contribution to aerosol optical closure remains uncertain. The high mass fraction of super-PM_{10} during episodic events suggests that excluding these particles leads to an underestimation of coarse-mode aerosol influences in climate models. The seasonal trends and episodic peaks observed in Figures 4 and 5, respectively emphasize the need for improved measurement techniques and better parameterization of coarse-mode aerosols in radiative forcing assessments.

4. Role of episodic variability

4.1 Optical and mass properties of PM_{10} aerosol particles at Hyytiälä: Episodic events and long-term trends

The optical and mass properties of PM_{10} aerosol particles at Hyytiälä exhibit variability influenced by episodic events and long-term trends. To classify the dominant aerosol types, we applied the framework by Cazorla et al. (2013), which utilizes the *SAE* and the *AAE*, as shown in Figure 6.

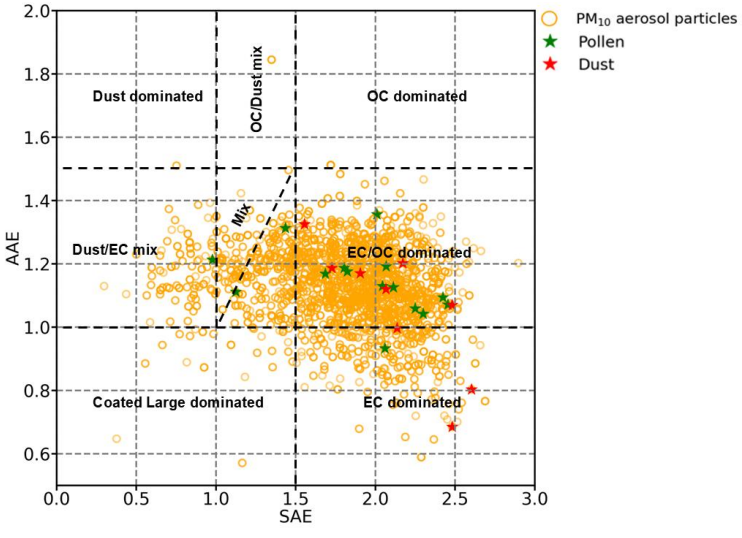

Figure 6. Aerosol classification matrix for the PM_{10} aerosol particles.

https://doi.org/10.5194/egusphere-2025-1776
Preprint. Discussion started: 13 May 2025

Figure 6 presents the aerosol classification for PM_{10} particles, which include both PM_1 and PM_{1-10} size fractions, thereby providing a broader perspective on aerosol interactions across size ranges. The data indicate that PM_{10} particles are predominantly located in the *EC/OC-dominated* and *Dust/EC mix* regions, suggesting substantial contributions from BC, SOA and aged mineral dust.

Pollen and dust events appear sporadically, clustering in moderate to high AAE and SAE regions, reinforcing their episodic nature. These events introduce short-term fluctuations in aerosol properties but do not significantly alter the long-term classification. Dust events cluster near the *'Dust/EC-dominated'* region, suggesting interactions between long-range transported dust and combustion aerosols. Pollen events align with higher *SAE* (~1.5–2), indicating smaller particles with strong scattering properties.

Despite episodic variability, the dominant aerosol classification remains stable, with PM_{10} aerosols primarily linked to EC/OC sources and aged dust.

Table 3 summarizes the classification scheme used in this study, differentiating aerosol types based on their optical properties:

(1) High *SAE* (>1.5) and low *AAE* (~1): BC-dominated aerosols from fossil fuel combustion and biomass burning.

(2) High *AAE* (>2) and low *SAE* (<1): Mineral dust, often associated with long-range transport.

(3) Intermediate *AAE* (1–2) and *SAE* (~1): Aged dust mixed with BC, indicative of interactions between transported dust and combustion aerosols.

Table 3. Summary of aerosol classifications in Figure 6.

Region in Figure 6	AAE	SAE	Size	Aerosol classification	Supporting studies
Dust Dominated	>2	<1	Coarse (>2.5 µm)	Mineral dust (e.g., desert regions)	Cazorla et al. (2013): *AAE* ~2.5, *SAE* ~0.5. Russell et al. (2010): Dust, coarse mode, high *AAE*. Malm and Hand (2007)**:** Dust from desert regions with low scattering efficiency.
Dust/EC Dominated	~1–2	~1	Mixed (fine + coarse)	Dust mixed with aged BC	Cazorla et al. (2013)**:** Mixed values for overlapping dust/BC. Clarke et al. (2007): Combustion aerosols interacting with dust.

https://doi.org/10.5194/egusphere-2025-1776
Preprint. Discussion started: 13 May 2025

EC Dominated	~1	>1.5	Fine (<1 µm)	Fossil fuel combustion (i.e. BC)	Schuster et al. (2006): *AAE* ~1 for BC. Clarke et al. (2007): *SAE* >1.5 for fine combustion aerosols. Sheridan and Ogren (1999): BC classification with low *AAE*.
OC Dominated	1.5–2	1–1.5	Fine to accumulation mode	Biomass burning, SOA	Cazorla et al. (2013): *AAE* ~1.8 for OC, moderate *SAE*. Russell et al. (2010): *AAE* 1.5–2 linked to OC. Malm and Hand (2007): OC from regional biomass burning or SOA formation.
Coated Large Dominated	<0	<0.5	Mixed/coarse	Aged aerosols, sulfate coating on dust	Malm and Hand (2007): Sulfate coating reduces *SAE* and *AAE*. Clarke et al. (2007): Coated particles with low *SAE*. Sheridan and Ogren (1999): Mixed aerosols with coatings.
Dust/OC or EC/OC Mixed	1–1.5	~1	Mixed (fine + coarse)	Mixed sources: urban, industrial, or forest	Cazorla et al. (2013): Mixed *AAE/SAE* values for overlapping sources. Clarke et al. (2007): Mixing of dust and pollution aerosols in urban environments. Malm and Hand (2007): Regional mixing.

4.2 Episodic and long-term variability: One-sided Mann-Whitney U test

To assess the impact of episodic events (i.e., pollen and dust) on aerosol properties, a one-sided Mann-Whitney U test was conducted. This non-parametric statistical test is particularly suited for comparing two independent datasets without assuming normality, making it effective for aerosol optical property distributions, which often exhibit non-Gaussian behavior due to episodic influences.

The dataset was categorized into:

https://doi.org/10.5194/egusphere-2025-1776
Preprint. Discussion started: 13 May 2025

(a) Observations including pollen and/or dust events

(b) Observations excluding these events

Pollen events were identified using cascade impactor filter records. If the PM_{10} filters contained pollen, the corresponding $PM_{1\text{-}10}$ fraction was also assumed to contain pollen.

Dust events were identified based on time periods from Varga et al. (2023), cross-referenced with aerosol optical and mass data from Hyytiälä.

Table 4. One-sided Mann-Whitney U-test results for the aerosol optical and mass properties in the presence of pollen and/or dust events for the $PM_{1–10}$ aerosol particles

Variable	Number of data points (pollen and/or dust events)	Number of data points (excluding pollen and /or dust events)	U-statistic	p-value	Statistical significance	Trend
$\sigma_{abs,520}$	29	3336	51394	0.56	No	No trend
$\sigma_{sca,550}$	30	3914	79862	6.63×10^{-4}	Yes	Increasing
PM mass	36	3626	94548	3.51×10^{-6}	Yes	Increasing
AAE	29	3254	66718	1.21×10^{-4}	Yes	Increasing
SAE	30	3880	52785	0.38	No	No trend
SSA_{550}	23	3174	28940	8.65×10^{-2}	No	No trend
MAC_{520}	29	2990	31641	1.22×10^{-2}	Yes	Decreasing
MSC_{550}	30	3515	38484	1.07×10^{-2}	Yes	Decreasing

Table 4 summarizes the statistical results. Statistically significant increases in $\sigma_{sca,550}$ (30 pseudo-daily mean values) were observed during identified pollen and/or dust events relative to periods without such events, indicating enhanced contributions from $PM_{1\text{-}10}$ particles to aerosol scattering.

Conversely, significant decrease in MAC_{520} (29 pseudo-daily mean values) suggest reductions in absorbing components and a shift toward smaller, more scattering aerosols. While PM_{10} particles primarily scatter light, mineral dust within this size range can also absorb radiation, influencing aerosol radiative properties (Adebiyi et al., 2023).

https://doi.org/10.5194/egusphere-2025-1776
Preprint. Discussion started: 13 May 2025

No significant trends were detected for SSA_{550} (23 pseudo-daily mean values), *AAE* (29 pseudo-daily mean values) or *SAE* (30 psudo-daily mean values). However, MAC_{520} exhibited a significant decreasing trend (29 psudo-daily mean values), suggesting a declining contribution from BC and other absorbing components. The stable SSA_{550} values, combined with declining MAC_{520}, indicate a shift toward aerosols with higher scattering-to-absorption ratios, likely due to increased sulfate or organic aerosol contributions.

Intensive properties also show variability during dust transport events, emphasizing the need to differentiate episodic contributions from long-term trends when interpreting radiative forcing estimates (Adebiyi et al., 2023; Che et al., 2018).

The aerosol classifications and trends observed in this study align with prior boreal aerosol research:

1. Virkkula et al. (2011) found that secondary organic aerosols (SOA) dominate boreal environments, with episodic pollen and dust events temporarily increasing coarse-mode contributions, aligning with the *'Dust-dominated'* and *'Dust/EC-dominated'* regions.

2. Hyvärinen et al. (2011) reported that long-range transported BC interacts with local aerosols, producing intermediate *AAE* values (~1–2), characteristic of the *'Dust/EC-dominated'* region.

3. Laing et al. (2016) emphasized the role of SOA and organic carbon aerosols from biomass burning in boreal forests, corresponding to the *'OC-dominated'* classification (*AAE* 1.5–2, *SAE* 1–1.5).

Coarse-mode aerosol measurements are affected by instrument-specific errors, such as angular truncation in nephelometers and artifacts in filter-based absorption techniques (Müller et al., 2011; Sheridan & Ogren, 1999). These uncertainties should be considered in climate models to improve estimates of aerosol–radiation interactions.

5. Summary and conclusions

This study provides new insights into the long-term evolution of aerosol optical properties and PM mass at the SMEAR II station in Hyytiälä, southern Finland, over the past 12 years. A significant decrease in extensive aerosol properties in PM_{10} aerosols suggests a shift in size distribution and chemical composition, likely driven by declining anthropogenic emissions, including SO_2, across northern Europe (Tørseth et al., 2012; Zieger et al., 2010). Seasonal patterns show that absorbing aerosols peak in winter due to biomass burning and residential heating, while scattering aerosols peak in summer, influenced by biogenic SOA formation and episodic pollen and dust events. These findings reinforce previous research on boreal aerosol processes and highlight the complex interactions between anthropogenic and natural aerosol sources at this site.

To address the challenge of incomplete optical closure, this study examines the role of supermicron aerosol particles across multiple seasons. The first-ever quantification of super-PM_{10} particles at Hyytiälä underscores their role in aerosol scattering and absorption processes, contributing to uncertainties in aerosol–radiation interactions. Statistical analysis revealed that pollen and dust events significantly affected five of the eight $PM_{1\text{-}10}$ aerosol optical and mass-related properties examined. The observed trends in MAC_{520} and MSC_{550} suggest changes in aerosol composition and size distribution, which must be considered in radiative forcing assessments. Future work should improve the representation of supermicron aerosols in climate models by leveraging advanced

https://doi.org/10.5194/egusphere-2025-1776
Preprint. Discussion started: 13 May 2025

analytical techniques, such as machine learning-based aerosol classification (Schuster et al., 2006) and integrating multi-platform observational datasets to reduce uncertainties.

Code/Data availability

The codes and data are available can be found at https://doi.org/10.5281/zenodo.15213383 (Banerji et al., 2025).

Author contributions

SB, KL and TP conceptualized the study. SB performed the data analysis. IY and LA contributed to the collection of data at SMEAR II. SB wrote the original draft and prepared the manuscript with input from KL. KL, IY, VMK and TP contributed to the review and revision of the manuscript, including the final edits. TP provided overall supervision and secured funding.

Competing interests

One of the co-authors is a member of the editorial board of *Atmospheric Chemistry and Physics*. This co-author had no involvement in the peer-review or editorial decision-making process for this manuscript. The authors declare no other competing interests.

Acknowledgements

The funding from ACTRIS-Finland host organizations University of Helsinki (UH) and INAR RI/ ACTRIS-FI 2020-2024 grant no. 328616, INAR RI 2022-2025 grant no. 345510 (UH), and the ACCC (Atmosphere and Climate Competence Center) Flagship funding by the Research Council of Finland (grant no. 337549 (UH) are gratefully acknowledged.

Support of the European Commission via non-CO_2 forcers and their climate, weather, air quality and health impacts (FOCI, project number 101056783) is gratefully acknowledged.

During the preparation of this work the authors used ChatGPT to improve the readability of certain sections. After using this tool, the authors reviewed and edited the content as needed and take full responsibility for the content of the manuscript.

References

Adebiyi, A., Kok, J. F., Murray, B. J., Ryder, C. L., Stuut, J.-B. W., Kahn, R. A., Knippertz, P., Formenti, P., Mahowald, N. M., Pérez García-Pando, C., Klose, M., Ansmann, A., Samset, B. H., Ito, A., Balkanski, Y., Di Biagio, C., Romanias, M. N., Huang, Y., & Meng, J. (2023). A review of coarse mineral dust in the Earth system. *Aeolian Research*, *60*, 100849. https://doi.org/https://doi.org/10.1016/j.aeolia.2022.100849

Äijälä, M., Daellenbach, K. R., Canonaco, F., Heikkinen, L., Junninen, H., Petäjä, T., Kulmala, M., Prévôt, A. S. H., & Ehn, M. (2019). Constructing a data-driven receptor model for organic and inorganic aerosol – a synthesis analysis of eight mass spectrometric data sets from a boreal forest site. *Atmospheric Chemistry and Physics*, *19*(6), 3645-3672. https://doi.org/10.5194/acp-19-3645-2019

https://doi.org/10.5194/egusphere-2025-1776
Preprint. Discussion started: 13 May 2025

Anderson, T. L., Covert, D. S., Marshall, S. F., Laucks, M. L., Charlson, R. J., Waggoner, A. P., Ogren, J. A., Caldow, R., Holm, R. L., Quant, F. R., Sem, G. J., Wiedensohler, A., Ahlquist, N. A., & Bates, T. S. (1996). Performance Characteristics of a High-Sensitivity, Three-Wavelength, Total Scatter/Backscatter Nephelometer. *Journal of Atmospheric and Oceanic Technology*, *13*(5), 967-986. https://doi.org/https://doi.org/10.1175/1520-0426(1996)013<0967:PCOAHS>2.0.CO;2

Anderson, T. L., & Ogren, J. A. (1998). Determining Aerosol Radiative Properties Using the TSI 3563 Integrating Nephelometer. *Aerosol Science and Technology*, *29*(1), 57-69. https://doi.org/10.1080/02786829808965551

Andreae, M. O., & Gelencsér, A. (2006). Black carbon or brown carbon? The nature of light-absorbing carbonaceous aerosols. *Atmos. Chem. Phys.*, *6*(10), 3131-3148. https://doi.org/10.5194/acp-6-3131-2006

Arnott, W. P., Khadeejeh, H., Hans, M., J., S. P., & and Ogren, J. A. (2005). Towards Aerosol Light-Absorption Measurements with a 7-Wavelength Aethalometer: Evaluation with a Photoacoustic Instrument and 3-Wavelength Nephelometer. *Aerosol Science and Technology*, *39*(1), 17-29. https://doi.org/10.1080/027868290901972

Arola, A., Schuster, G., Myhre, G., Kazadzis, S., Dey, S., & Tripathi, S. N. (2011). Inferring absorbing organic carbon content from AERONET data. *Atmospheric Chemistry and Physics*, *11*(1), 215-225. https://doi.org/10.5194/acp-11-215-2011

Backman, J., Schmeisser, L., Virkkula, A., Ogren, J. A., Asmi, E., Starkweather, S., Sharma, S., Eleftheriadis, K., Uttal, T., Jefferson, A., Bergin, M., Makshtas, A., Tunved, P., & Fiebig, M. (2017). On Aethalometer measurement uncertainties and an instrument correction factor for the Arctic. *Atmos. Meas. Tech.*, *10*(12), 5039-5062. https://doi.org/10.5194/amt-10-5039-2017

Bali, K., Banerji, S., Campbell, J. R., Bhakta, A. V., Chen, L. W. A., Holmes, C. D., & Mao, J. (2024). Measurements of brown carbon and its optical properties from boreal forest fires in Alaska summer. *Atmospheric Environment*, *324*, 120436-120436. https://doi.org/https://doi.org/10.1016/j.atmosenv.2024.120436

Banerji, S., Luoma, K., Ylivinkka, I., Ahonen, L., Kerminen, V.-M., & Petäjä, T. (2025). *Data for "Measurement Report: Optical properties of supermicron aerosol particles in a boreal environment", Zenodo [data set]* https://doi.org/https://doi.org/10.5281/zenodo.15213383

Bates, T. S., Quinn, P. K., Coffman, D. J., Johnson, J. E., & Middlebrook, A. M. (2005). Dominance of organic aerosols in the marine boundary layer over the Gulf of Maine during NEAQS 2002 and their role in aerosol light scattering. *Journal of Geophysical Research: Atmospheres*, *110*(D18). https://doi.org/https://doi.org/10.1029/2005JD005797

Bergstrom, R. W., Pilewskie, P., Russell, P. B., Redemann, J., Bond, T. C., Quinn, P. K., & Sierau, B. (2007). Spectral absorption properties of atmospheric aerosols. *Atmos. Chem. Phys.*, *7*(23), 5937-5943. https://doi.org/10.5194/acp-7-5937-2007

Bernardoni, V., Ferrero, L., Bolzacchini, E., Forello, A. C., Gregorič, A., Massabò, D., Močnik, G., Prati, P., Rigler, M., Santagostini, L., Soldan, F., Valentini, S., Valli, G., & Vecchi, R. (2021). Determination of Aethalometer multiple-scattering enhancement parameters and impact on source apportionment during the winter 2017/18 EMEP/ACTRIS/COLOSSAL campaign in Milan. *Atmos. Meas. Tech.*, *14*(4), 2919-2940. https://doi.org/10.5194/amt-14-2919-2021

Berner, A., & Luerzer, C. (1980). Mass size distributions of traffic aerosols at Vienna. *The Journal of Physical Chemistry*, *84*(16), 2079-2083. https://doi.org/10.1021/j100453a016

Bond, T. C., & Bergstrom, R. W. (2006). Light Absorption by Carbonaceous Particles: An Investigative Review. *Aerosol Science and Technology*, *40*(1), 27-67. https://doi.org/10.1080/02786820500421521

Bond, T. C., Doherty, S. J., Fahey, D. W., Forster, P. M., Berntsen, T., Deangelo, B. J., Flanner, M. G., Ghan, S., Kärcher, B., Koch, D., Kinne, S., Kondo, Y., Quinn, P. K., Sarofim, M. C., Schultz, M. G., Schulz, M., Venkataraman, C., Zhang, H., Zhang, S., . . . Zender, C. S. (2013). Bounding the

role of black carbon in the climate system: A scientific assessment. *Journal of Geophysical Research Atmospheres*, *118*(11), 5380-5552. https://doi.org/10.1002/jgrd.50171

Boy, M. (2004). Overview of the field measurement campaign in Hyytiala, August 2001 in the frame of the EU project OSOA (vol 4, pg 657, 2004). *Atmospheric Chemistry and Physics*, *4*, 1739-1739. http://www.copernicus.org/EGU/EGU.html

Brasseur, Z., Castarède, D., Thomson, E. S., Adams, M. P., Drossaart van Dusseldorp, S., Heikkilä, P., Korhonen, K., Lampilahti, J., Paramonov, M., Schneider, J., Vogel, F., Wu, Y., Abbatt, J. P. D., Atanasova, N. S., Bamford, D. H., Bertozzi, B., Boyer, M., Brus, D., Daily, M. I., . . . Duplissy, J. (2022). Measurement report: Introduction to the HyICE-2018 campaign for measurements of ice-nucleating particles and instrument inter-comparison in the Hyytiälä boreal forest. *Atmospheric Chemistry and Physics*, *22*(8), 5117-5145. https://doi.org/10.5194/acp-22-5117-2022

Brasseur, Z., Schneider, J., Lampilahti, J., Vakkari, V., & Sinclair, V. A. (2024). Vertical distribution of ice nucleating particles over the boreal forest of Hyytiälä , Finland. 11305-11332.

Cappa, C. D., Kolesar, K. R., Zhang, X., Atkinson, D. B., Pekour, M. S., Zaveri, R. A., Zelenyuk, A., & Zhang, Q. (2016). Understanding the optical properties of ambient sub-and supermicron particulate matter: Results from the CARES 2010 field study in northern California. *Atmospheric Chemistry and Physics*, *16*(10), 6511-6535. https://doi.org/10.5194/acp-16-6511-2016

Cazorla, A., Bahadur, R., Suski, K. J., Cahill, J. F., Chand, D., Schmid, B., Ramanathan, V., & Prather, K. A. (2013). Relating aerosol absorption due to soot, organic carbon, and dust to emission sources determined from in-situ chemical measurements. *Atmospheric Chemistry and Physics*, *13*(18), 9337-9350. https://doi.org/10.5194/acp-13-9337-2013

Che, H., Qi, B., Zhao, H., Xia, X., Eck, T. F., Goloub, P., Dubovik, O., Estelles, V., Cuevas-Agulló, E., Blarel, L., Wu, Y., Zhu, J., Du, R., Wang, Y., Wang, H., Gui, K., Yu, J., Zheng, Y., Sun, T., . . . Zhang, X. (2018). Aerosol optical properties and direct radiative forcing based on measurements from the China Aerosol Remote Sensing Network (CARSNET) in eastern China. *Atmos. Chem. Phys.*, *18*(1), 405-425. https://doi.org/10.5194/acp-18-405-2018

Clarke, A., McNaughton, C., Kapustin, V., Shinozuka, Y., Howell, S., Dibb, J., Zhou, J., Anderson, B., Brekhovskikh, V., Turner, H., & Pinkerton, M. (2007). Biomass burning and pollution aerosol over North America: Organic components and their influence on spectral optical properties and humidification response. *Journal of Geophysical Research: Atmospheres*, *112*(D12). https://doi.org/https://doi.org/10.1029/2006JD007777

Collaud Coen, M., Andrews, E., Lastuey, A., Petkov Arsov, T., Backman, J., Brem, B. T., Bukowiecki, N., Couret, C., Eleftheriadis, K., Flentje, H., Fiebig, M., Gysel-Beer, M., Hand, J. L., Hoffer, A., Hooda, R., Hueglin, C., Joubert, W., Keywood, M., Eun Kim, J., . . . Laj, P. (2020). Multidecadal trend analysis of in situ aerosol radiative properties around the world. *Atmospheric Chemistry and Physics*, *20*(14), 8867-8908. https://doi.org/10.5194/acp-20-8867-2020

Collaud Coen, M., Weingartner, E., Apituley, A., Ceburnis, D., Fierz-Schmidhauser, R., Flentje, H., Henzing, J. S., Jennings, S. G., Moerman, M., Petzold, A., Schmid, O., & Baltensperger, U. (2010). Minimizing light absorption measurement artifacts of the Aethalometer: evaluation of five correction algorithms. *Atmos. Meas. Tech.*, *3*(2), 457-474. https://doi.org/10.5194/amt-3-457-2010

Després, V. R., Huffman, J. A., Burrows, S. M., Hoose, C., Safatov, A. S., Buryak, G., Fröhlich-Nowoisky, J., Elbert, W., Andreae, M. O., Pöschl, U., & Jaenicke, R. (2012). Primary biological aerosol particles in the atmosphere: a review. *Tellus B: Chemical and Physical Meteorology*, *64*(1). https://doi.org/10.3402/tellusb.v64i0.15598

Drinovec, L., Močnik, G., Zotter, P., Prévôt, A. S. H., Ruckstuhl, C., Coz, E., Rupakheti, M., Sciare, J., Müller, T., Wiedensohler, A., & Hansen, A. D. A. (2015). The "dual-spot" Aethalometer: an improved measurement of aerosol black carbon with real-time loading compensation. *Atmos. Meas. Tech.*, *8*(5), 1965-1979. https://doi.org/10.5194/amt-8-1965-2015

https://doi.org/10.5194/egusphere-2025-1776
Preprint. Discussion started: 13 May 2025

Ehn, M., Thornton, J. A., Kleist, E., Sipilä, M., Junninen, H., Pullinen, I., Springer, M., Rubach, F., Tillmann, R., Lee, B., Lopez-Hilfiker, F., Andres, S., Acir, I.-H., Rissanen, M., Jokinen, T., Schobesberger, S., Kangasluoma, J., Kontkanen, J., Nieminen, T., . . . Mentel, T. F. (2014). A large source of low-volatility secondary organic aerosol. *Nature*, *506*(7489), 476-479. https://doi.org/10.1038/nature13032

Emerson, E. W., Hodshire, A. L., DeBolt, H. M., Bilsback, K. R., Pierce, J. R., McMeeking, G. R., & Farmer, D. K. (2020). Revisiting particle dry deposition and its role in radiative effect estimates. *Proceedings of the National Academy of Sciences*, *117*(42), 26076-26082. https://doi.org/10.1073/pnas.2014761117

Guenther, A., Karl, T., Harley, P., Wiedinmyer, C., Palmer, P. I., & Geron, C. (2006). Estimates of global terrestrial isoprene emissions using MEGAN (Model of Emissions of Gases and Aerosols from Nature). *Atmos. Chem. Phys.*, *6*(11), 3181-3210. https://doi.org/10.5194/acp-6-3181-2006

Hakola, H., Tarvainen, V., Laurila, T., Hiltunen, V., Hellén, H., & Keronen, P. (2003). Seasonal variation of VOC concentrations above a boreal coniferous forest. *Atmospheric Environment*, *37*(12), 1623-1634. https://doi.org/10.1016/s1352-2310(03)00014-1

Hallquist, M., Wenger, J. C., Baltensperger, U., Rudich, Y., Simpson, D., Claeys, M., Dommen, J., Donahue, N. M., George, C., Goldstein, A. H., Hamilton, J. F., Herrmann, H., Hoffmann, T., Iinuma, Y., Jang, M., Jenkin, M. E., Jimenez, J. L., Kiendler-Scharr, A., Maenhaut, W., . . . Wildt, J. (2009). The formation, properties and impact of secondary organic aerosol: current and emerging issues. *Atmos. Chem. Phys.*, *9*(14), 5155-5236. https://doi.org/10.5194/acp-9-5155-2009

Hari, P., & Kulmala, M. (2005). Station for Measuring Ecosystem-Atmosphere Relations (SMEAR II). *Boreal Environment Research*, *10*, 315-322. https://www.borenv.net/BER/archive/pdfs/ber10/ber10-315.pdf

Hari, P., Nikinmaa, E., Pohja, T., Siivola, E., Bäck, J., Vesala, T., & Kulmala, M. (2013). Station for measuring ecosystem-atmosphere relations: SMEAR. *Physical and Physiological Forest Ecology*, *9789400756*(October), 471-487. https://doi.org/10.1007/978-94-007-5603-8_9

Heikkinen, L., Äijälä, M., Daellenbach, K. R., Chen, G., Garmash, O., Aliaga, D., Graeffe, F., Räty, M., Luoma, K., Aalto, P., Kulmala, M., Petäjä, T., Worsnop, D., & Ehn, M. (2021). Eight years of sub-micrometre organic aerosol composition data from the boreal forest characterized using a machine-learning approach. *Atmospheric Chemistry and Physics*, *21*(13), 10081-10109. https://doi.org/10.5194/acp-21-10081-2021

Heikkinen, L., Äijälä, M., Riva, M., Luoma, K., Dällenbach, K., Aalto, J., Aalto, P., Aliaga, D., Aurela, M., Keskinen, H., Makkonen, U., Rantala, P., Kulmala, M., Petäjä, T., Worsnop, D., & Ehn, M. (2020). Long-term sub-micrometer aerosol chemical composition in the boreal forest: inter- and intra-annual variability. *Atmospheric Chemistry and Physics*, *20*(5), 3151-3180. https://doi.org/10.5194/acp-20-3151-2020

Hellén, H., Dommen, J., Metzger, A., Gascho, A., Duplissy, J., Tritscher, T., Prevot, A. S. H., & Baltensperger, U. (2008). Using Proton Transfer Reaction Mass Spectrometry for Online Analysis of Secondary Organic Aerosols. *Environmental Science & Technology*, *42*(19), 7347-7353. https://doi.org/10.1021/es801279m

Hienola, A. I., Pietikäinen, J. P., Jacob, D., Pozdun, R., Petäjä, T., Hyvärinen, A. P., Sogacheva, L., Kerminen, V. M., Kulmala, M., & Laaksonen, A. (2013). Black carbon concentration and deposition estimations in Finland by the regional aerosol–climate model REMO-HAM. *Atmospheric Chemistry and Physics*, *13*(8), 4033-4055. https://doi.org/10.5194/acp-13-4033-2013

Hyvärinen, A. P., Kolmonen, P., Kerminen, V. M., Virkkula, A., Leskinen, A., Komppula, M., Hatakka, J., Burkhart, J., Stohl, A., Aalto, P., Kulmala, M., Lehtinen, K. E. J., Viisanen, Y., & Lihavainen, H. (2011). Aerosol black carbon at five background measurement sites over Finland, a gateway

to the Arctic. *Atmospheric Environment*, *45*(24), 4042-4050. https://doi.org/https://doi.org/10.1016/j.atmosenv.2011.04.026

Kourtchev, I., Giorio, C., Manninen, A., Wilson, E., Mahon, B., Aalto, J., Kajos, M., Venables, D., Ruuskanen, T., Levula, J., Loponen, M., Connors, S., Harris, N., Zhao, D., Kiendler-Scharr, A., Mentel, T., Rudich, Y., Hallquist, M., Doussin, J.-F., . . . Kalberer, M. (2016). Enhanced Volatile Organic Compounds emissions and organic aerosol mass increase the oligomer content of atmospheric aerosols. *Scientific Reports*, *6*(1), 35038. https://doi.org/10.1038/srep35038

Kukkonen, J., López-Aparicio, S., Segersson, D., Geels, C., Kangas, L., Kauhaniemi, M., Maragkidou, A., Jensen, A., Assmuth, T., Karppinen, A., Sofiev, M., Hellén, H., Riikonen, K., Nikmo, J., Kousa, A., Niemi, J. V., Karvosenoja, N., Sousa Santos, G., Sundvor, I., . . . Brandt, J. (2020). The influence of residential wood combustion on the concentrations of PM2.5 in four Nordic cities. *Atmospheric Chemistry and Physics*, *20*(7), 4333-4365. https://doi.org/10.5194/acp-20-4333-2020

Kulmala, M., Hämeri, K., Aalto, P. P., Mäkelä, J. M., Pirjola, L., Douglas Nilsson, E., Buzorius, G., Rannik, Ü., Dal Maso, M., Seidl, W., Hoffman, T., Janson, R., Hansson, H. C., Viisanen, Y., Laaksonen, A., & O'Dowd, C. D. (2001). Overview of the international project on biogenic aerosol formation in the boreal forest (BIOFOR). *Tellus, Series B: Chemical and Physical Meteorology*, *53*(4), 324-343. https://doi.org/10.3402/tellusb.v53i4.16601

Laakso, L., Grönholm, T., Rannik, Ü., Kosmale, M., Fiedler, V., Vehkamäki, H., & Kulmala, M. (2003). Ultrafine particle scavenging coefficients calculated from 6 years field measurements. *Atmospheric Environment*, *37*(25), 3605-3613. https://doi.org/https://doi.org/10.1016/S1352-2310(03)00326-1

Lack, D. A., & Cappa, C. D. (2010). Impact of brown and clear carbon on light absorption enhancement, single scatter albedo and absorption wavelength dependence of black carbon. *Atmos. Chem. Phys.*, *10*(9), 4207-4220. https://doi.org/10.5194/acp-10-4207-2010

Laing, J. R., Jaffe, D. A., & Hee, J. R. (2016). Physical and optical properties of aged biomass burning aerosol from wildfires in Siberia and the Western USA at the Mt. Bachelor Observatory. *Atmos. Chem. Phys.*, *16*(23), 15185-15197. https://doi.org/10.5194/acp-16-15185-2016

Laj, P., Myhre, C. L., Riffault, V., Amiridis, V., Fuchs, H., Eleftheriadis, K., Petäjä, T., Salameh, T., Kivekäs, N., Juurola, E., Saponaro, G., Philippin, S., Cornacchia, C., Arboledas, L. A., Baars, H., Claude, A., De Mazière, M., Dils, B., Dufresne, M., . . . Vana, M. (2024). Aerosol, Clouds and Trace Gases Research Infrastructure (ACTRIS): The European Research Infrastructure Supporting Atmospheric Science. *Bulletin of the American Meteorological Society*, *105*(7), E1098-E1136. https://doi.org/10.1175/BAMS-D-23-0064.1

Laskin, A., Iedema, M. J., Ichkovich, A., Graber, E. R., Taraniuk, I., & Rudich, Y. (2005). Direct observation of completely processed calcium carbonate dust particles [10.1039/B417366J]. *Faraday Discussions*, *130*(0), 453-468. https://doi.org/10.1039/B417366J

Latimer, R. N. C., & Martin, R. V. (2019). Interpretation of measured aerosol mass scattering efficiency over North America using a chemical transport model. *Atmospheric Chemistry and Physics*, *19*(4), 2635-2653. https://doi.org/10.5194/acp-19-2635-2019

Leskinen, A., Arola, A., Komppula, M., Portin, H., Tiitta, P., Miettinen, P., Romakkaniemi, S., Laaksonen, A., & Lehtinen, K. E. J. (2012). Seasonal cycle and source analyses of aerosol optical properties in a semi-urban environment at Puijo station in Eastern Finland. *Atmospheric Chemistry and Physics*, *12*(12), 5647-5659. https://doi.org/10.5194/acp-12-5647-2012

Lihavainen, H., Hyvärinen, A., Asmi, E., Hatakka, J., & Viisanen, Y. (2015). Long-term variability of aerosol optical properties in northern Finland. *Boreal Environment Research*, *20*(4), 526-541.

Liousse, C., Cachier, H., & Jennings, S. G. (1993). Optical and thermal measurements of black carbon aerosol content in different environments: Variation of the specific attenuation cross-section, sigma (σ). *Atmospheric Environment Part A, General Topics*, *27*(8), 1203-1211. https://doi.org/10.1016/0960-1686(93)90246-U

https://doi.org/10.5194/egusphere-2025-1776
Preprint. Discussion started: 13 May 2025

Luoma, K., Virkkula, A., Aalto, P., Lehtipalo, K., Petäjä, T., & Kulmala, M. (2021). Effects of different correction algorithms on absorption coefficient – a comparison of three optical absorption photometers at a boreal forest site. *Atmos. Meas. Tech.*, *14*(10), 6419-6441. https://doi.org/10.5194/amt-14-6419-2021

Luoma, K., Virkkula, A., Aalto, P., Petäjä, T., & Kulmala, M. (2019). Over a 10-year record of aerosol optical properties at SMEAR II. *Atmospheric Chemistry and Physics*, *19*(17), 11363-11382. https://doi.org/10.5194/acp-19-11363-2019

Mahowald, N., Albani, S., Kok, J. F., Engelstaeder, S., Scanza, R., Ward, D. S., & Flanner, M. G. (2014). The size distribution of desert dust aerosols and its impact on the Earth system. *Aeolian Research*, *15*, 53-71. https://doi.org/10.1016/j.aeolia.2013.09.002

Malm, W. C., & Hand, J. L. (2007). An examination of the physical and optical properties of aerosols collected in the IMPROVE program. *Atmospheric Environment*, *41*(16), 3407-3427. https://doi.org/https://doi.org/10.1016/j.atmosenv.2006.12.012

Manninen, H. E., Bäck, J., Sihto-Nissilä, S.-L., Huffman, J. A., Pessi, A.-M., Hiltunen, V., Aalto, P. P., Hidalgo, P. J., Hari, P., Saarto, A., Kulmala, M., & Petäjä, T. (2014). Patterns in airborne pollen and other primary biological aerosol particles (PBP), and their contribution to aerosol mass and number in a boreal forest. *Boreal Environment Research*, *19*, 383-405. https://helda.helsinki.fi/server/api/core/bitstreams/f1408a0d-26ad-4b3d-91bc-db8b0e8e603a/content

Maso, M. D., Kulmala, M., Riipinen, I., Wagner, R., Hussein, T., Aalto, P. P., & Lehtinen, K. E. J. (2005). Formation and growth of fresh atmospheric aerosols: eight years of aerosol size distribution data from SMEAR II, Hyytiälä, Finland. *Boreal Environment Research*, *10*, 323–336.

McFiggans, G., Artaxo, P., Baltensperger, U., Coe, H., Facchini, M. C., Feingold, G., Fuzzi, S., Gysel, M., Laaksonen, A., Lohmann, U., Mentel, T. F., Murphy, D. M., O'Dowd, C. D., Snider, J. R., & Weingartner, E. (2006). The effect of physical and chemical aerosol properties on warm cloud droplet activation. *Atmos. Chem. Phys.*, *6*(9), 2593-2649. https://doi.org/10.5194/acp-6-2593-2006

Moosmüller, H., Chakrabarty, R. K., & Arnott, W. P. (2009). Aerosol light absorption and its measurement: A review. *Journal of Quantitative Spectroscopy and Radiative Transfer*, *110*(11), 844-878. https://doi.org/https://doi.org/10.1016/j.jqsrt.2009.02.035

Müller, T., Henzing, J. S., de Leeuw, G., Wiedensohler, A., Alastuey, A., Angelov, H., Bizjak, M., Collaud Coen, M., Engström, J. E., Gruening, C., Hillamo, R., Hoffer, A., Imre, K., Ivanow, P., Jennings, G., Sun, J. Y., Kalivitis, N., Karlsson, H., Komppula, M., . . . Wang, Y. Q. (2011). Characterization and intercomparison of aerosol absorption photometers: result of two intercomparison workshops. *Atmospheric Measurement Techniques*, *4*(2), 245-268. https://doi.org/10.5194/amt-4-245-2011

Pandolfi, M., Alados-Arboledas, L., Alastuey, A., Andrade, M., Angelov, C., Artiñano, B., Backman, J., Baltensperger, U., Bonasoni, P., Bukowiecki, N., Collaud Coen, M., Conil, S., Coz, E., Crenn, V., Dudoitis, V., Ealo, M., Eleftheriadis, K., Favez, O., Fetfatzis, P., . . . Laj, P. (2018). A European aerosol phenomenology – 6: scattering properties of atmospheric aerosol particles from 28 ACTRIS sites. *Atmos. Chem. Phys.*, *18*(11), 7877-7911. https://doi.org/10.5194/acp-18-7877-2018

Pandolfi, M., Ripoll, A., Querol, X., & Alastuey, A. (2014). Climatology of aerosol optical properties and black carbon mass absorption cross section at a remote high-altitude site in the western Mediterranean Basin. *Atmospheric Chemistry and Physics*, *14*(12), 6443-6460. https://doi.org/10.5194/acp-14-6443-2014

Petäjä, T., Järvi, L., Kerminen, V. M., Ding, A. J., Sun, J. N., Nie, W., Kujansuu, J., Virkkula, A., Yang, X., Fu, C. B., Zilitinkevich, S., & Kulmala, M. (2016). Enhanced air pollution via aerosol-boundary layer feedback in China. *Scientific Reports*, *6*(July 2015), 1-6. https://doi.org/10.1038/srep18998

Petäjä, T., Tabakova, K., Manninen, A., Ezhova, E., O'Connor, E., Moisseev, D., Sinclair, V. A., Backman, J., Levula, J., Luoma, K., Virkkula, A., Paramonov, M., Räty, M., Äijälä, M., Heikkinen, L., Ehn, M., Sipilä, M., Yli-Juuti, T., Virtanen, A., . . . Kerminen, V. M. (2022). Influence of biogenic emissions from boreal forests on aerosol–cloud interactions. *Nature Geoscience*, *15*(1), 42-47. https://doi.org/10.1038/s41561-021-00876-0

Petäjä, T., Ylivinkka, I., Kokkonen, T., Schiestl-Aalto, P., Kerminen, V.-M., Bäck, J., & Kulmala, M. (2025). Chapter 15 - Air quality and the environmental impacts. In R. S. Sokhi (Ed.), *Air Quality* (pp. 439-462). Elsevier. https://doi.org/https://doi.org/10.1016/B978-0-12-822591-2.00015-9

Petzold, A., Schloesser, H., Sheridan, P. J., Arnott, W. P., Ogren, J. A., & Virkkula, A. (2005). Evaluation of multiangle absorption photometry for measuring aerosol light absorption. *Aerosol Science and Technology*, *39*(1), 40-51. https://doi.org/10.1080/027868290901945

Petzold, A., & Schönlinner, M. (2004). Multi-angle absorption photometry - A new method for the measurement of aerosol light absorption and atmospheric black carbon. *Journal of Aerosol Science*, *35*(4), 421-441. https://doi.org/10.1016/j.jaerosci.2003.09.005

Rantala, P., Aalto, J., Taipale, R., Ruuskanen, T. M., & Rinne, J. (2015). Annual cycle of volatile organic compound exchange between a boreal pine forest and the atmosphere. *Biogeosciences*, *12*(19), 5753-5770. https://doi.org/10.5194/bg-12-5753-2015

Russell, P. B., Bergstrom, R. W., Shinozuka, Y., Clarke, A. D., DeCarlo, P. F., Jimenez, J. L., Livingston, J. M., Redemann, J., Dubovik, O., & Strawa, A. (2010). Absorption Angstrom Exponent in AERONET and related data as an indicator of aerosol composition. *Atmos. Chem. Phys.*, *10*(3), 1155-1169. https://doi.org/10.5194/acp-10-1155-2010

Saturno, J., Pöhlker, C., Massabò, D., Brito, J., Carbone, S., Cheng, Y., Chi, X., Ditas, F., Hrab De Angelis, I., Morán-Zuloaga, D., Pöhlker, M. L., Rizzo, L. V., Walter, D., Wang, Q., Artaxo, P., Prati, P., & Andreae, M. O. (2017). Comparison of different Aethalometer correction schemes and a reference multi-wavelength absorption technique for ambient aerosol data. *Atmospheric Measurement Techniques*, *10*(8), 2837-2850. https://doi.org/10.5194/amt-10-2837-2017

Schneider, J., Höhler, K., Heikkilä, P., Keskinen, J., Bertozzi, B., Bogert, P., Schorr, T., Umo, N. S., Vogel, F., Brasseur, Z., Wu, Y., Hakala, S., Duplissy, J., Moisseev, D., Kulmala, M., Adams, M. P., Murray, B. J., Korhonen, K., Hao, L., . . . Möhler, O. (2021). The seasonal cycle of ice-nucleating particles linked to the abundance of biogenic aerosol in boreal forests. *Atmospheric Chemistry and Physics*, *21*(5), 3899-3918. https://doi.org/10.5194/acp-21-3899-2021

Schuster, G. L., Dubovik, O., & Holben, B. N. (2006). Angstrom exponent and bimodal aerosol size distributions. *Journal of Geophysical Research Atmospheres*, *111*(7), 1-14. https://doi.org/10.1029/2005JD006328

Seinfeld, J. H., & Pandis, S. N. (2016). *Atmospheric Chemistry and Physics: From Air Pollution to Climate Change*. Wiley. https://books.google.fi/books?id=n_RmCgAAQBAJ

Sheridan, P. J., & Ogren, J. A. (1999). Observations of the vertical and regional variability of aerosol optical properties over central and eastern North America. *Journal of Geophysical Research Atmospheres*, *104*(D14), 16793-16805. https://doi.org/10.1029/1999JD900241

Smith, S. J., Van Aardenne, J., Klimont, Z., Andres, R. J., Volke, A., & Delgado Arias, S. (2011). Anthropogenic sulfur dioxide emissions: 1850-2005. *Atmospheric Chemistry and Physics*, *11*(3), 1101-1116. https://doi.org/10.5194/acp-11-1101-2011

Tian, P., Yu, Z., Cui, C., Huang, J., Kang, C., Shi, J., Cao, X., & Zhang, L. (2023). Atmospheric aerosol size distribution impacts radiative effects over the Himalayas via modulating aerosol single-scattering albedo. *npj Climate and Atmospheric Science*, *6*(1). https://doi.org/10.1038/s41612-023-00368-5

Titos, G., Burgos, M. A., Zieger, P., Alados-Arboledas, L., Baltensperger, U., Jefferson, A., Sherman, J., Weingartner, E., Henzing, B., Luoma, K., O'Dowd, C., Wiedensohler, A., & Andrews, E. (2021).

A global study of hygroscopicity-driven light-scattering enhancement in the context of other in situ aerosol optical properties. *Atmospheric Chemistry and Physics*, *21*(17), 13031-13050. https://doi.org/10.5194/acp-21-13031-2021

Tørseth, K., Aas, W., Breivik, K., Fjæraa, A. M., Fiebig, M., Hjellbrekke, A. G., Lund Myhre, C., Solberg, S., & Yttri, K. E. (2012). Introduction to the European Monitoring and Evaluation Programme (EMEP) and observed atmospheric composition change during 1972–2009. *Atmos. Chem. Phys.*, *12*(12), 5447-5481. https://doi.org/10.5194/acp-12-5447-2012

Tunved, P., Hansson, H. C., Kerminen, V. M., Ström, J., Dal Maso, M., Lihavainen, H., Viisanen, Y., Aalto, P. P., Komppula, M., & Kulmala, M. (2006). High natural aerosol loading over boreal forests. *Science*, *312*(5771), 261-263. https://doi.org/10.1126/science.1123052

van de Hulst, H. C. (1980). *Multiple Light Scattering*. Academic Press. https://doi.org/https://doi.org/10.1016/B978-0-12-710701-1.X5001-0

Varga, G., Meinander, O., Rostási, Á., Dagsson-Waldhauserova, P., Csávics, A., & Gresina, F. (2023). Saharan, Aral-Caspian and Middle East dust travels to Finland (1980–2022). *Environment International*, *180*(September). https://doi.org/10.1016/j.envint.2023.108243

Virkkula, A., Backman, J., Aalto, P. P., Hulkkonen, M., Riuttanen, L., Nieminen, T., Dal Maso, M., Sogacheva, L., De Leeuw, G., & Kulmala, M. (2011). Seasonal cycle, size dependencies, and source analyses of aerosol optical properties at the SMEAR II measurement station in Hyytiälä, Finland. *Atmospheric Chemistry and Physics*, *11*(9), 4445-4468. https://doi.org/10.5194/acp-11-4445-2011

Weingartner, E., Saathoff, H., Schnaiter, M., Streit, N., Bitnar, B., & Baltensperger, U. (2003). Absorption of light by soot particles: Determination of the absorption coefficient by means of aethalometers. *Journal of Aerosol Science*, *34*(10), 1445-1463. https://doi.org/10.1016/S0021-8502(03)00359-8

Yli-Panula, E., Fekedulegn, D. B., Green, B. J., & Ranta, H. (2009). Analysis of airborne Betula pollen in Finland; a 31-year perspective. *International Journal of Environmental Research and Public Health*, *6*(6), 1706-1723. https://doi.org/10.3390/ijerph6061706

Zhang, L., Gong, S., Padro, J., & Barrie, L. (2001). A size-segregated particle dry deposition scheme for an atmospheric aerosol module. *Atmospheric Environment*, *35*(3), 549-560. https://doi.org/https://doi.org/10.1016/S1352-2310(00)00326-5

Zieger, P., Aalto, P. P., Aaltonen, V., Äijälä, M., Backman, J., Hong, J., Komppula, M., Krejci, R., Laborde, M., Lampilahti, J., De Leeuw, G., Pfüller, A., Rosati, B., Tesche, M., Tunved, P., Väänänen, R., & Petäjä, T. (2015). Low hygroscopic scattering enhancement of boreal aerosol and the implications for a columnar optical closure study. *Atmospheric Chemistry and Physics*, *15*(13), 7247-7267. https://doi.org/10.5194/acp-15-7247-2015

Zieger, P., Fierz-Schmidhauser, R., Gysel, M., Ström, J., Henne, S., Yttri, K. E., Baltensperger, U., & Weingartner, E. (2010). Effects of relative humidity on aerosol light scattering in the Arctic. *Atmos. Chem. Phys.*, *10*(8), 3875-3890. https://doi.org/10.5194/acp-10-3875-2010

Zotter, P., Herich, H., Gysel, M., El-Haddad, I., Zhang, Y., Mocnik, G., Hüglin, C., Baltensperger, U., Szidat, S., & Prévôt, A. S. H. (2017). Evaluation of the absorption Ångström exponents for traffic and wood burning in the Aethalometer-based source apportionment using radiocarbon measurements of ambient aerosol. *Atmospheric Chemistry and Physics*, *17*(6), 4229-4249. https://doi.org/10.5194/acp-17-4229-2017